Northumbria
University
NEWCASTLE

JOURNAL OF GEOPHYSICAL RESEARCH: OCEANS, VOL. 118, 6603–6620, doi:10.1002/2013JC008871, 2013

Variability of Circumpolar Deep Water transport onto the Amundsen Sea continental shelf through a shelf break trough

K. M. Assmann,[1] A. Jenkins,[1] D. R. Shoosmith,[1] D. P. Walker,[1] S. S. Jacobs,[2] and K. W. Nicholls[1]

Received 22 February 2013; revised 30 September 2013; accepted 4 October 2013; published 6 December 2013.

[1] The presence of warm Circumpolar Deep Water (CDW) intrusions on the Amundsen continental shelf has been linked to recent thinning of the outlet glaciers draining the West Antarctic ice sheet into the Amundsen Sea. Inflow of the CDW onto the shelf is thought to occur within a series of troughs that intersect the continental shelf break. We use observations between 1994 and 2011 and a numerical model to investigate the variability of CDW transport in a trough intersecting the shelf break at 113°W. The location of the main CDW inflow into the trough varies between its eastern flank and center, while the western part of the trough is filled by a recirculation that commonly entrains cooler water originating further south on the shelf. Thermocline depth decreases between the early and late 2000s with an indication that the depth of the 1994 thermocline was similar to the later years. Mooring results show that the CDW layer cools and thins in summer and thickens and warms in winter. In addition to a deeper thermocline in summer, we observe a stronger presence of Lower CDW in the bottom of the trough. Heat flux onto the shelf is controlled by current velocities rather than CDW temperature and the majority of the heat is carried onto the shelf by background flow rather than episodic events.

Citation: Assmann, K. M., A. Jenkins, D. R. Shoosmith, D. P. Walker, S. S. Jacobs, and K. W. Nicholls (2013), Variability of Circumpolar Deep Water transport onto the Amundsen Sea continental shelf through a shelf break trough, *J. Geophys. Res. Oceans*, *118*, 6603–6620, doi:10.1002/2013JC008871.

1. Introduction and Background

[2] The continental shelves of the Antarctic marginal seas form the interface between the Antarctic ice sheet and the surrounding ocean. The majority of the mass loss from the ice sheet to the ocean is divided between calving icebergs and melting from the base of floating ice shelves. The rate of basal melting is influenced by the shape of the sub-ice shelf cavities, the temperature of seawater that enters them, and the access that water has to the ice, particularly near deep grounding lines. The temperature of seawater in the ice shelf cavities is controlled by that of water masses that cross the shelf break and by subsequent processes on the continental shelf.

[3] Circumpolar Deep Water (CDW) is the main source of oceanic heat in the Southern Ocean. In the Weddell and Ross Seas, where there are large cyclonic polar gyres seaward of the continental shelves, CDW is cooled within the gyres and by mixing near the shelf break and associated slope front. Once on the continental shelf more heat can be extracted by overturning during vigorous sea ice formation. Flowing into the large cavities beneath the Ross and Filchner and Ronne Ice Shelves, the cold, dense shelf water causes melting of a few tens of centimeter per year due to the pressure dependence of the freezing point [*Jacobs et al*., 1996; *Nicholls et al*., 2009; *Rignot et al*., 2013].

[4] By contrast, the warmer CDW along the SE Pacific continental shelf break is not significantly modified during its passage across a weak slope front and continental shelf toward the ice shelf cavities [*Hellmer et al*., 1998; *Walker et al*., 2007; *Moffat et al*., 2009; *Jenkins et al*., 2010; *Jacobs et al*., 2011]. In the Amundsen Sea, some of those ice shelves extend >1000 m below sea level. This can result in their exposure to seawater with temperatures up to 4°C above the in situ melting point, and basal melt rates orders of magnitude higher than beneath the large ice shelves [*Jacobs et al*., 1996; *Rignot and Jacobs*, 2002; *Rignot et al*., 2013]. In addition, observations of outlet glaciers reaching the Amundsen Sea show that this region is experiencing the largest thinning rates on the Antarctic ice sheet [*Shepherd et al*., 2001; *Zwally et al*., 2005; *Rignot et al*., 2008; *Pritchard et al*., 2009; *Wingham et al*., 2009] likely resulting from reduced ice shelf buttressing as basal melting increased [*Jenkins et al*., 2010; *Jacobs et al*., 2011].

[5] For a long time, the Amundsen Sea was one of the most scarcely sampled regions of the Southern Ocean because of its remoteness and thick perennial sea ice cover. Oceanographic observations on the Amundsen continental shelf started in 1994 and have greatly increased in frequency over the past decade.

[1]British Antarctic Survey, Cambridge, UK.
[2]Lamont-Doherty Earth Observatory, Columbia University, Palisades, New York, USA.

Corresponding author: K. M. Assmann, British Antarctic Survey, High Cross, Madingley Road, Cambridge CB3 0ET, UK. (kmassmann22@gmail.com)

2169-9275/13/10.1002/2013JC008871

[6] The inflow of CDW onto the Amundsen shelf has been found to be linked to a series of depressions in the shelf break bathymetry (Figure 1). A shelf break depression that intersects the shelf break near 118°W deepens southward and leads to the Dotson and Getz ice shelves [*Wåhlin et al*., 2010], while two features further east at 113°W and 102–108°W merge on the shelf and represent the main access path for CDW into the Pine Island Embayment [*Hellmer et al*., 1998; *Thoma et al*., 2008; *Jacobs et al*., 2011; *Schodlok et al*., 2012]. *Walker et al*. [2007] presented observations from a 2003 section across the trough at 113°W. They showed that it was filled with CDW below 400 m with sufficient heat to sustain a significant portion of ice shelf basal melting in Pine Island Bay.

[7] The results of a series of idealized modeling studies of the effect of a shelf break canyon on on-shelf flow imply that the direction of the along-shelf flow is crucial for facilitating transport of water onto the shelf [*Klinck*, 1996]. In the Southern Hemisphere, the interaction of right-bounded flow with the canyon carries water onto the shelf. In the case of the Antarctic shelf seas, this corresponds to eastward flow. In the Bellingshausen Sea, the eastward Antarctic Circumpolar Current (ACC) hugs the shelf break and seawater with temperatures up to 1.8°C is found on the shelf [*Orsi et al*., 1995; *Moffat et al*., 2009; *Martinson and McKee*, 2012]. By contrast, a series of sections across the continental shelf break from the 2003 Amundsen Sea cruise confirm that the Southern Antarctic Circumpolar Current Front (SACCF) is located well north of the shelf break at 113°W [*Walker et al*., 2013, hereafter referred to as *W13*]. Circulation in this area appears to be part of a recirculation at the eastern end of the Ross Gyre. However, geostrophic velocities on the sections show generally westward flow at the surface that overlies a strong eastward undercurrent at the shelf break [*W13*]. The interaction of the latter with the 113°W shelf break depression is thought to facilitate CDW transport onto the Amundsen shelf. Using an idealized numerical model to investigate wind-driven slope currents, *Middleton and Cirano* [1999] found that an eastward bottom intensified undercurrent emerges in a downwelling system, i.e., a westward shelf break current driven by easterlies in the Southern Hemisphere. Such an undercurrent is initially (10–20 days) set up by coastal trapped waves and later maintained by a combination of thermal wind shear (southward tilt of the isopycnals at the slope front) and a bottom mixed layer. The Amundsen shelf break lies within the band of coastal easterlies from November to June (Figure 1a) helping to establish such an eastward undercurrent. In winter, the westerlies shift southward over the shelf break and likely induce an eastward shift of flow over the full water column, further enhancing the undercurrent. *Thoma et al*. [2008] argue that westerly winds over the shelf break also aid CDW transport onto the shelf.

[8] We will focus here on the inflowing CDW once it has entered the shelf through the shelf break depression which intersects the Amundsen shelf break at 113°W, for which oceanographic observations exist from two *RRS James Clark Ross* cruises, three *RVIB Nathaniel B. Palmer* cruises, and one *RVIB Oden* cruise, spanning 1994–2009, as well as a mooring from February 2009 to January 2011 (Figure 1b). These observations provide the opportunity to assess inflow variability on daily to annual time scales, to investigate the processes governing inflow variability and to discuss the implications for heat transport to the deep grounding lines of the ice shelves bordering Pine Island Bay.

2. Data and Methods

2.1. Observational Database

[9] This study is mainly based on two cruises conducted on *RRS James Clark Ross* in March 2003 and February 2006, and mooring BSR12 which was deployed in early 2009 and recovered in January 2011. We supplement these with scattered stations from *RVIB Nathaniel B. Palmer* cruises in 1994, 2000, and 2009. In addition, we used stations taken during a late 2008 cruise on *RVIB Oden*. The cruises, and their dates are summarized in Table 1. Figure 1b shows the location of the hydrographic stations and the mooring within the trough. Mooring BSR12 was deployed in a water depth of 611 m on 12 February 2009 and recovered on 8 January 2011 at 71.57°S, 113.04°W. Depths and IDs of instruments are summarized in Table 2.

[10] To reference the geostrophic transports calculated from the two cross-trough sections taken during the 2003 and 2006 cruises, we used Ship-board Acoustic Doppler Current Profiler (SADCP) data and largely followed the method employed by W13. SADCP data were detided and averaged for each station and for the periods of steady steaming between stations. N-S and E-W velocity components were rotated to calculate the cross-section (along-trough) velocity. Geostrophic velocities were referenced to the mean SADCP current between 100 and 300 m. Please refer to Appendix A for details of the detiding and referencing method.

2.2. Model

[11] To illustrate the flow pattern within the trough, we use a regional setup of MITgcm that includes a sea ice model [*Losch et al*., 2010] and the sub-ice shelf-ocean interaction [*Losch*, 2008]. The model domain is 80°W to 140°W and 76°S to 62°S with a resolution of 0.1° longitude and 0.1° × cos (ϕ) latitude. This corresponds to approximately 3.5 km in the trough area which is close to the magnitude of the internal Rossby radius (5.4 km) at the shelf break. The model has 50 layers in the vertical of which 20 are located in the top 1000 m. We used bathymetry and ice shelf thickness from RTOPO1.0.5 [*Timmermann et al*., 2010] and the NCEP Climate Forecast System Reanalysis (CFSR) [*Saha et al*., 2010] at 6 hourly resolution as atmospheric forcing. Vertical mixing is parameterized by the K-profile Parameterization (KPP) scheme of *Large et al*. [1994]. Tides are not included in the model. The model is initialized from rest with World Ocean Atlas 2009 (WOA09) potential temperature [*Locarnini et al*., 2010] and salinity [*Antonov et al*., 2010]. A mean annual cycle in monthly means of WOA09 potential temperature and salinity is prescribed at the open boundaries. A mean annual cycle of monthly mean velocities is prescribed at the boundaries from a circumpolar setup of MITgcm that was run at 0.25° resolution with the same atmospheric forcing (P. Holland, personal communication, 2011). The sea ice model is run with closed boundaries, after sensitivity studies

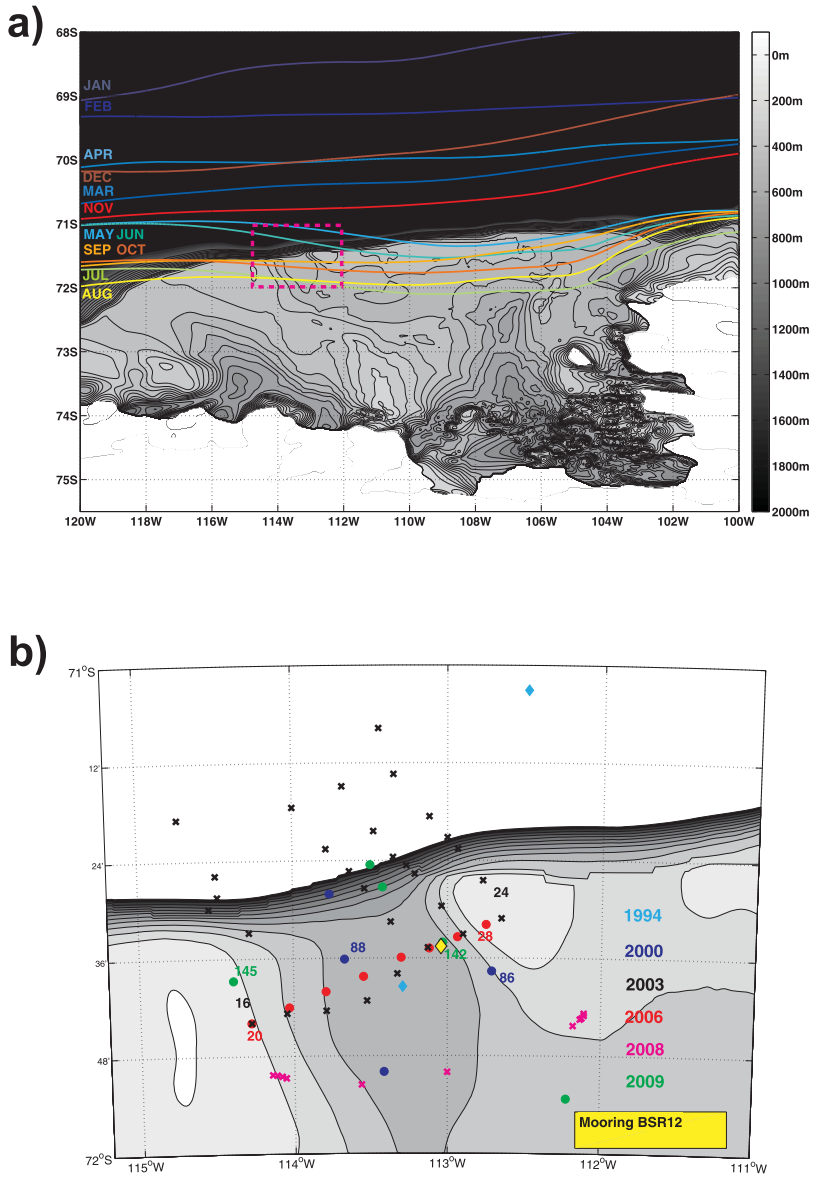

Figure 1. (a) Map of the Amundsen Sea. Bathymetry (shaded) taken from RTOPO1.0.5 [*Timmermann et al.*, 2010]. Black contour lines are every 100 m for depths between 1500 and 700 m and every 50 m between 700 and 150 m depth. The colored contour lines are the zero contours, i.e., the boundary between easterlies and westerlies, for each month of the mean annual cycle of zonal winds from CFSR 1979–2011. The magenta rectangle indicates the 113°W trough area. (b) Map of the 113°W trough as indicated by the magenta rectangle in Figure 1a with the observations color-coded according to the legend.

indicated that drift velocities would have to be prescribed at daily or shorter time scales to have an impact on the model interior due to the fast response of sea ice to winds. As a result, we underestimate winter sea ice extent due to the missing import of sea ice at the western boundary, but there do not appear to be any artificially low or high salinities at the boundaries due to the short relaxation time scale (1–5 days) to the hydrographic boundary conditions. The model is spun-up for 10 years using NCEP CFSR year 1980 and then run from 1979 to 2011.

3. Results

[12] The late summer temperature and salinity profiles in the 113°W outer shelf depression suggest interannual variability of a similar magnitude as has been found on the inner shelf [*Jacobs et al.*, 2011, 2013]. Near the sea surface a shallow halocline separates fresh Antarctic Surface Water (AASW) from colder and saltier Winter Water (WW), in turn separated from the CDW by a broad thermocline (Figure 2).

[13] Temperatures in the AASW layer only exceeded −1.5°C in February 2006. AASW salinities vary by nearly 1.0 psu, and mixed layer depths range from 15 to 40 m. The lower extent of the underlying WW layer varies in depth from <150 m in 2006 to >300m in 2000. The WW layer is not strictly isothermal with temperatures above the surface freezing point and weakly increasing salinities with depth. The depth of the thermocline and halocline connecting the WW and CDW also varied by ≈150 m at these

Table 1. Summary of Cruises Used for This Study[a]

Cruise Year	Cruise ID	Cruise Dates	Trough Station Dates
1994	NBP9402	14 Feb 1994 to 5 Apr1994	7 Mar
2000	NBP0001	15 Feb 2000 to 1 Apr2000	11–12 Mar
2003	JR84	28 Feb 2003 to 4 Apr 2003	16–23 Mar
2006	JR141	8 Jan 2006 to 22 Feb 2006	7–8 Feb
2008	ODO0809	10 Dec 2008 to 7 Jan 2009	16–17 Dec
2009	NBP0901	5 Jan 2009 to 28 Feb 2009	12–13 Feb

[a]The table gives the cruise year which we will use as reference to the cruise in this study, the original cruise ID, the cruise dates, and the dates of stations occupied in the 113°W trough.

profile sites and times with deeper thermoclines in 2000 and 2003 and shallower ones in 1994, 2006, and 2009. Apart from this temporal variability, the thermocline between WW and CDW shoals from west to east within the depression (Figure 3).

[14] The CDW temperature maximum (T_{max}) is located between 400 and 450 m in all years, i.e., roughly at the depth of the shallower bathymetry on each side of the depression (Figure 3). It does not exceed 1.5°C on either the E-W sections or Figure 2 profiles, reaching values of 1.45°C near 113.2°W in 2003 and 1.31°C at 112.9°W and 1.39°C at 113.8°W in 2006. *Orsi et al*. [1995] use the 1.7°C isotherm to mark the SACCF and consequently the southern extent of Upper Circumpolar Deep Water (UCDW). The CDW temperature maximum is therefore not strictly UCDW, but its relatively high temperatures and low oxygen values (4.3 mL/L, available for the N.B. Palmer cruises) suggest it is a southward extension of this water mass. Salinities increasing to 34.725 and temperatures decreasing to values around 1°C in the bottom of the trough identify these waters as Lower Circumpolar Deep Water (LCDW) [*Orsi et al*., 1995]. Fresher (34.6) waters with temperatures below 1°C were found at the western end of the 2003 section, and extended eastward near the seafloor beneath the warm core. A similar gradient in temperature and salinity across the depression was encountered along the December 2008 section further south in the trough, and in February 2009 later that austral summer (Figure 2).

[15] Based on these summer profiles, thermohaline variability in the depression is largest in the thermocline and in the depth of the bottom of the overlying WW layer. There are no obvious temporal trends in those features, nor do their fluctuations appear to correlate with variability of the CDW T_{max} (Figure 2).

[16] As described in section 2 and Appendix, we reference geostrophic velocities from the 2003 and 2006 sections using various methods to detide and average the SADCP data from the same cruises (Figures A2 and A3). While current magnitudes differ, the shear is similar regardless of referencing method and we therefore show the mean over all methods in Figure 3. In 2003, the main inflow is located in the trough center with velocities of 0.08 ± 0.02 m s^{-1} on the western side of the warm, salty UCDW core. The error interval represents the standard deviation of the different referencing and detiding methods. Velocities in the eastern part of the trough are weak and may form a weak recirculation (Figure 3). To the west, a recirculation pattern consists of an outflow between stations 19 and 20 and inflow farther west, overlain by an outflow core in the thermocline and WW. In 2006, a similar pattern appears on the western side of the section, with a weaker secondary inflow. The main inflow hugs the eastern flank of the trough with a core velocity of 0.11 ± 0.04 m s^{-1}.

[17] Surface referenced geostrophic transport of CDW (neutral density >28.0) [*Whitworth et al*., 1998] onto the shelf is 25% larger in 2006 than in 2003 (Table 3). Using the undetided SADCP data for referencing, the total on-shelf CDW transport is virtually identical for the two years. When tides are taken into account, on-shelf CDW transport is enhanced for 2003, while it is reduced for 2006 for all detiding methods. Despite large differences in the tidal ellipses used in the different detiding methods (Figure A1, Appendix), the resulting transports are reasonably consistent, especially in 2003 if the top mooring current meter (211 MAB. MAB is meters above bottom.) estimate is ignored. Tidal currents around the trough are generally small (0.01–0.04 m s^{-1}, W13), but these results imply that they are large enough to impact the use of synoptic sections to estimate changes in on-shelf CDW transport on interannual time scales.

[18] Mooring BSR12 was located at 71.58°S, 113.04°W on the cross-trough section between February 2009 and January 2011 (Figure 1b). This places it in the main CDW inflow core for 2006 and in its eastern extension for 2003 (Figure 3). The deployed instruments cover the CDW layer and the base of the thermocline (Table 2 and Figure 2). Mean February and March temperatures for 2009 and 2010 are close to those from the 2009 CTD stations and the spread in mooring temperatures for those months is similar in magnitude to the interannual variability within the CDW layer (Figure 2). Interannual temperature variability in the

Table 2. Summary of Instruments, Their Depths, and Quantities Measured on Mooring BSR12 at 71.57°S, 113.04°W[a]

Instrument ID	Depth (m)	MAB	Variables Measured
AEM36	400	211	T,U,V
SBE39_4545	450	161	T,P
SBE39_4544	502	99	T,P
AQD3322	553	58	T,U,V,P
SBE37_6423	580	31	T,S,P

[a]MAB is meters above bottom, T is temperature, S is salinity, U is zonal velocity component (positive eastward), V is meridional velocity component (positive northward), and P is pressure. AEM stands for Alec Electromagnetic current meter, AQD for Nortek Aquadopp current meter, and SBE are Seabird Electronics microcats.

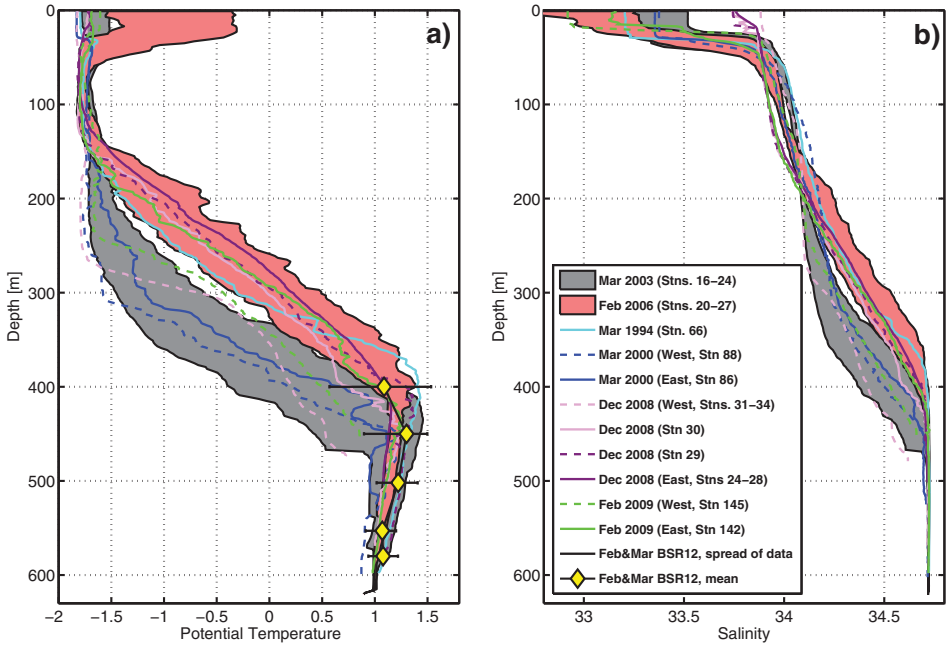

Figure 2. (a) Temperature and (b) salinity profiles for stations close to the cross-trough sections. Stations used were station 66 for 1994 (cyan), 86 (blue solid), and 88 (blue dashed) for 2000, 16–24 for 2003 (gray shaded), 20–27 for 2006 (red shaded), 24–34 for 2008 (pink and purple), and 142 (green solid) and 145 (green dashed) for 2009. For the 2003 and 2006 sections, the shaded areas mark the minimum and maximum temperature and salinity for the 8 stations on the cross-trough section at each depth level. Yellow diamonds in Figure 2a mark the mean February and March temperatures on mooring BSR12 with black bars indicating the spread of the temperatures during those months.

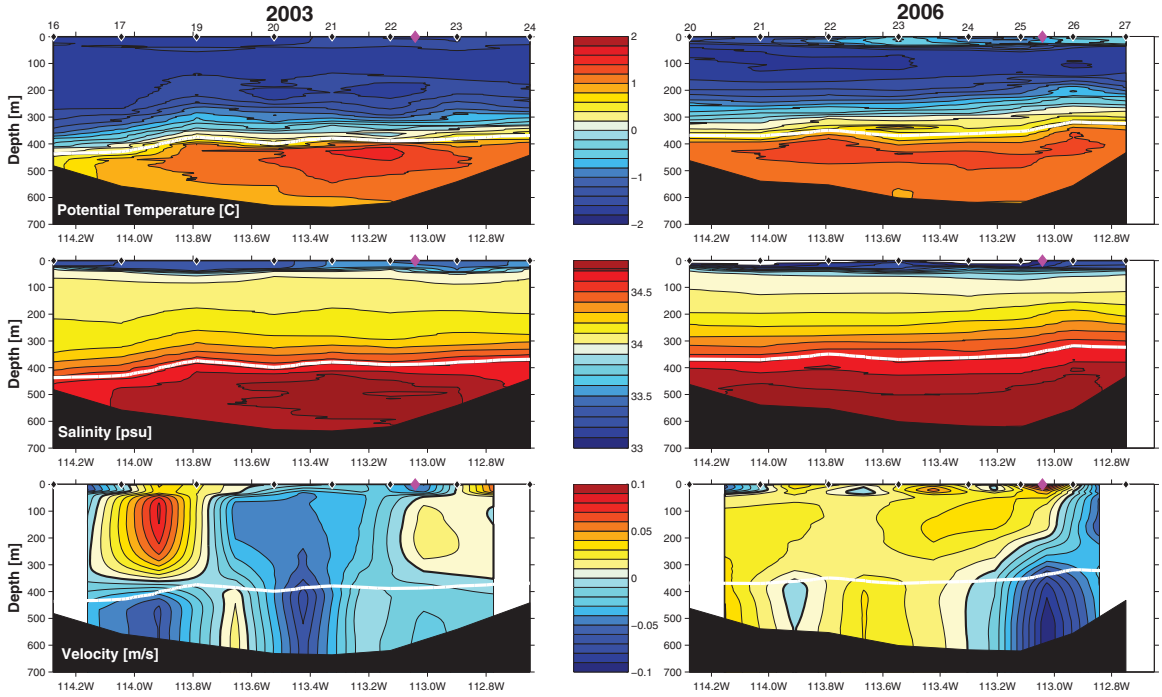

Figure 3. For the cross-trough sections occupied during 2003 (left) and 2006 (right), from the (top) Potential temperature, salinity, and the mean of the referenced cross-section geostrophic velocities (positive off the shelf, negative onto the shelf) shown in Figures A2 and A3 in Appendix. Neutral density $\gamma_n = 28.0$ is marked in white, stations are marked as black diamonds, and mooring BSR12 in magenta. Bottom triangles between stations are filled using a constant shear approach.

Table 3. Transport of CDW (Neutral Density >28.0) Through the 113°W Trough[a]

Reference	2003	2006
Surface referenced	−237	−297
ADCP (not detided)	−177 ± 102	−161 ± 42
ADCP(CATS detided)	−256 ± 107	67 ± 39
ADCP (*Allen* combined detided)	−209 ± 104	−114 ± 41
ADCP (*Allen* single detided)	−218 ± 106	−137 ± 37
ADCP (BSR12 58MAB detided)	−282 ± 103	−38 ± 41
ADCP (BSR12 211MAB detided)	−511 ± 103	−108 ± 39

[a]Negative values denote transport onto the shelf, positive ones the opposite. All transports in mSv (10^3 m^3 s^{-1}).

lower thermocline exceeds the variability observed over the 2 years of the mooring data.

[19] The mooring temperature time series (Figure 4) show that the depression was filled with CDW for the entire deployment period and the temperature structure within the CDW was retained throughout. The temperatures at 31 MAB and 58 MAB covary closely ($r = 0.95$ for the raw time series) and are generally about 0.2°C cooler than those at 99 MAB which is at the lower edge of the T_{max} core and 161 MAB which is located within this core with temperatures reaching up to 1.55°C. The sensor at 211 MAB has the largest temperature variability with temperatures ranging from 0.4°C to 1.6°C. Most peak temperatures at 211 MAB are nearly identical with those at 161 MAB suggesting that the T_{max} core thickens intermittently, particularly in winter. The temperature minima at 211 MAB occur in spring and summer and indicate deepening of the thermocline. All temperature series show a similar seasonal cycle of warm autumn and winter and cold spring and summer with an earlier onset of the cooling in 2010.

[20] Mean velocities at both current meter depths are directed southward into the trough with 0.07 ± 0.11 m s^{-1} at 211 MAB and 0.05 ± 0.05 m s^{-1} at 58 MAB after detiding them using T_TIDE (*Pawlowicz et al*. [2002], updated 2011). Error intervals are the standard deviation of the time series. Current variability near the base of the thermocline (Figure 5c) was higher at short time scales than that in the CDW layer (Figure 5d). We applied a Singular Spectrum Analysis (SSA) [*Vautard et al*., 1992] to the mooring time series to separate the signal into statistically independent components, allowing us to identify the dominant components of variability at weekly to monthly time scales shown as black lines in Figure 5. Current variability at longer time scales is shown to be largely barotropic between the two instrument depths by the SSA with a correlation coefficient $r = 0.85$ for principal component 1 (PC1) of the two time series. The correlation between temperature and inflow velocity is weak and not statistically significant in the thermocline ($r = 0.05$ for the 2 hourly series and $r = 0.18$ for PC1) and weak, but significant at the 95% level in the CDW layer ($r = 0.29$ for the hourly time series and $r = 0.34$ for PC1). Note that stronger inflow is negative and that lower temperatures therefore correlate with a stronger inflow.

[21] We calculated heat fluxes relative to the surface freezing point for both 211 and 58 MAB (Figure 5). Calculating heat fluxes referenced to the surface freezing point makes them comparable between depths and provides a lower bound on the melting potential this water would have, were it to interact with an ice shelf base unmodified. Variability of the heat flux is dominated by the variability in velocity, since temperatures at both depths are warm in comparison with the surface freezing point. The mean heat flux at 58 MAB, 0.62 MW m^{-2} directed onto the shelf, is ≈67% of that at 211 MAB (0.89 MW m^{-2}) over the 694 day records, close to the ratio of their mean velocities.

[22] Along-trough velocities at 58 MAB are close to normally distributed, but show a higher proportion of strong inflow velocities than expected that we interpret as events of stronger inflow (Figures 6a and 6b). The most prominent of these occurs in August 2010 (Figures 5c and 5d). The events of strong inflow are associated with lower CDW temperatures (Figure 6c). To estimate the importance of the

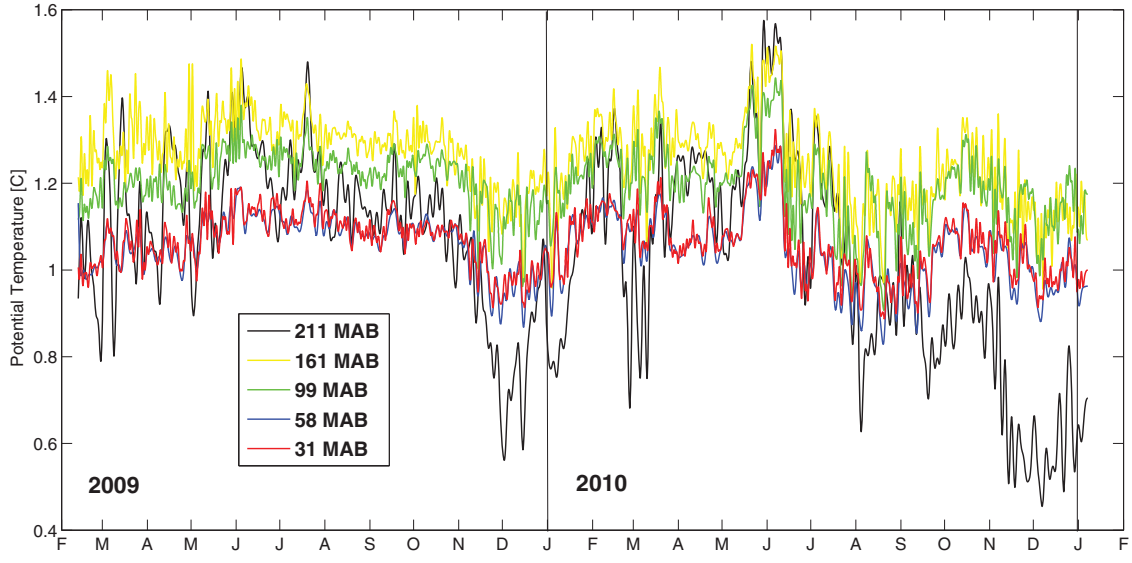

Figure 4. Two day low-pass filtered potential temperature time series for all depths on mooring BSR12 (71.58°S, 113.04°W, Figure 1b). MAB denotes meters above bottom which was at 611 m.

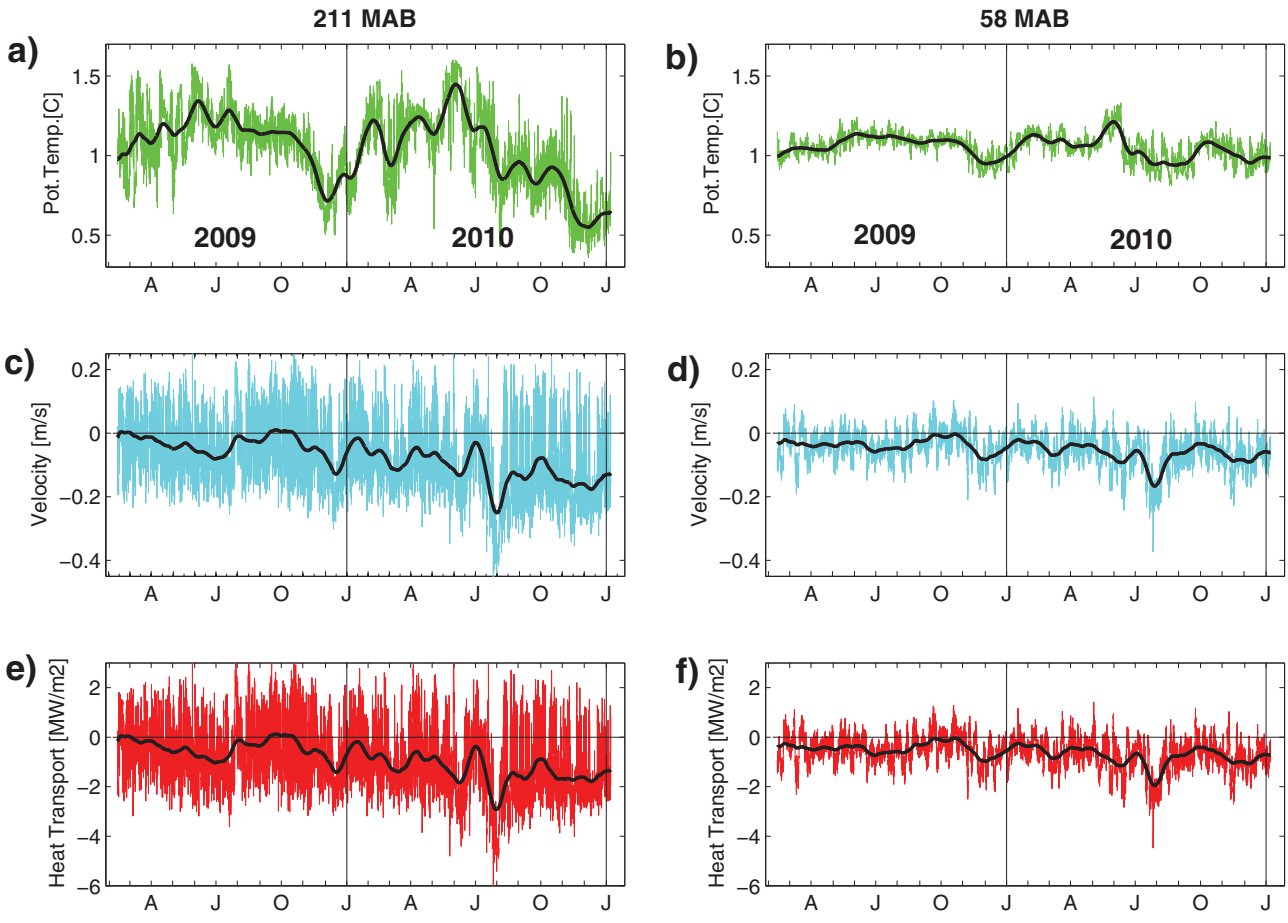

Figure 5. Time series for the mooring temperature sensors and current meters: Potential temperature (°C), (a) 211 MAB, (b) 58 MAB. Along-trough velocity (m s^{-1}), (c) 211 MAB, (d) 58 MAB. Heat transport w.r.t. surface point freezing temperature (MW m^{-2}), (e) 211 MAB, (f) 58 MAB. Negative (positive) velocities and heat transports are directed onto (off) the continental shelf. Velocities were detided with T_TIDE (*Pawlowicz et al*. [2002], updated 2011). Colored lines show the original data at 2 h resolution. The black lines show principal component 1 (PC1) of a Singular Spectrum Analysis (SSA) [*Vautard et al*., 1992]. The variance explained by PC1 is 98% (99%), 48% (66%), and 46% (66%) for temperature, velocity, and heat transport, respectively (numbers in brackets are for 58 MAB).

events for the on-shelf heat transport, we defined them as those periods when velocities at 58 MAB are below −0.1 m s^{-1}, where more negative velocities indicate stronger on-shelf flow. This is the point below which the observed velocity distribution consistently exceeds the expected normal distribution (Figures 6a and 6b). To obtain an estimate of the robustness of the results, we varied the cut-off velocity from −0.08 to −0.12 m s^{-1} and error intervals given represent the standard deviation for this set of values.

[23] Events of strong on-shelf flow at 58 MAB occur for 10 ± 4% of the mooring deployment period. The mean heat flux onto the shelf during these events is almost four times larger than for the background flow (1.85 ± 0.18 MW m^{-2} versus 0.49 ± 0.04 MW m^{-2}). However, when we consider the total amount of heat transported onto the shelf during the BSR12 deployment period, we find that only about 30% of the total heat is transported onto the shelf during events ($1.08 \pm 0.33 \times 10^{13}$ J m^{-2} versus $2.63 \pm 0.34 \times 10^{13}$ J m^{-2}). This implies that background flow carries the majority of heat onto the shelf during the deployment period of the mooring.

[24] Salinity was only measured at 31 MAB on the mooring. At time scales >2 days, salinities are positively correlated with temperature throughout the 2 year record increasing in winter and decreasing in summer (Figure 7). When plotted on a Θ-S diagram, Θ-S properties follow the mixing line between the LCDW salinity maximum and the cooler and fresher deep water lower on the continental slope (Figure 8). Water filling the bottom of the depression has characteristics closer to the deep water in summer and LCDW in winter. Toward winter 2010 temperatures recover to the same levels as 2009, but salinities stay about 0.004 psu fresher. The early part of the mooring record agrees with the 2006 and 2009 Θ-S characteristics, while the fresher water seen in 2010 lies within the range of the 2003 cross-trough section (Figure 8).

[25] In mid-June of 2010, directly after the warmest period in the record, a downward drift in salinity is unmatched by a corresponding temperature decline (Figure 7). Water mass characteristics then match those of the lower thermocline above the T_{max} which might have been expected if, e.g., a deep mixing event entrained lower thermocline water

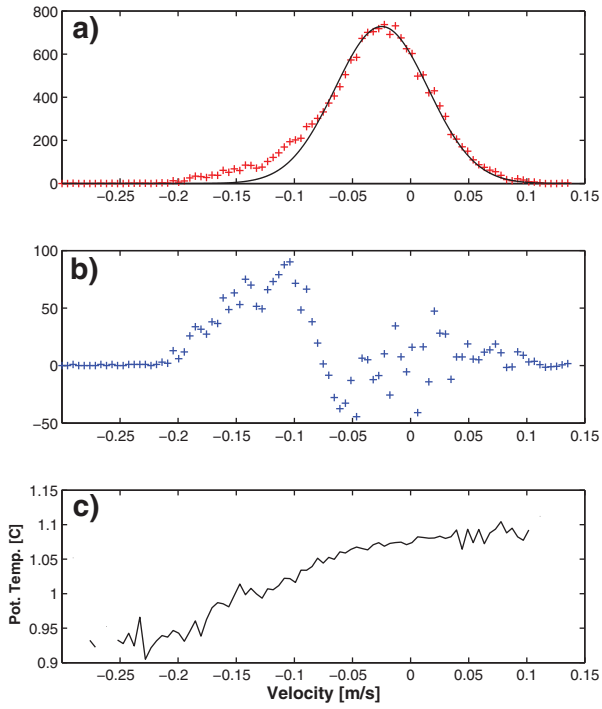

Figure 6. (a) Histogram of the hourly cross-section velocities for the current meter 58 MAB (blue crosses) and a Gaussian fit to the distribution. The velocity time series was detrended using a second-order polynomial fit for this purpose. (b) Difference between the distribution of cross-section velocities for 58 MAB and the Gaussian fit. (c) Potential temperature as a function of cross-section velocity for 58 MAB. Negative (positive) velocities are directed onto (off) the continental shelf. Velocities were detided with T_TIDE (*Pawlowicz et al*. [2002], updated 2011).

(note the 211 MAB record in Figure 4). However, Figure 4 shows that the water column structure of a clear T_{max} between 99 and 161 MAB is retained throughout the latter part of the record and the occurrence of such an event is thus unlikely. In addition, a post-recovery CTD cast gave a salinity of ≈34.72 at the 580 m depth of this instrument, further indicating anomalous, nonlinear sensor drift. The portion of the salinity record plotted in gray thus seems doubtful, but has been retained in Figure 8, as water with similar Θ-S properties at comparable depths has been observed further west along the Amundsen shelf break (cf. N.B. Palmer 2009 cruise, station 157).

4. Comparison with Model Results

[26] We use our model results to illustrate the horizontal structure of the circulation in the 113°W trough. Model sections across the trough, along the observed 2003 and 2006 sections, show that the model reproduces the general water mass distribution in the trough (Figures 9a and 9b). The gradient toward lower temperatures and salinities (not shown) at the western end of the trough appears to be a permanent feature in the model results. While the T_{max} in the center of the CDW layer is not apparent in the cross-trough sections (Figures 9a and 9b), a time series of potential temperature profiles at the mooring position (71.57°S, 113.04°W) shows that the model does reproduce this feature, but about 50 m too high in the water column (Figures 10a and 10b). The comparison to the observed mooring temperatures indicates that the entire CDW layer is too thick and too warm in the model. The model reproduces the thinning and cooling of the CDW layer in January and February 2010 and shows a shoaling thermocline and warmer T_{max} cores in autumn. In the model, this shoaling of the thermocline does not persist through winter as in the observations due to overestimated winter mixing.

[27] Modeled cross-section velocities clearly show a main inflow in the eastern part of the trough (Figures 9c and 9d). The 75 m thick model layer centered at 522.5 m shown in Figures 9e and 9f covers the center of the CDW layer. The current pattern in this layer illustrates how the eastward undercurrent hugging the shelf break turns south into the eastern part of the trough. A small anticyclonic circulation of varying strength exists in the model north of the trough mouth. A tongue of warmer water extends eastward along its southern limb and may offer an explanation for the warm water lenses seen in the 2003 cross-shelf sections (*W13*, their Figure 6).

[28] The model CDW inflow is located between the more central position of the observed 2003 section and the eastern one of the 2006 inflow and does not shift position significantly over time (Figures 9c and 9d). The magnitude of the simulated inflow velocities (Figure 10c) compares well to observations, but smaller temporal variability at the mooring location may be attributed to this lack of spatial variability of the inflow. This indicates that smaller-scale processes, not represented in the model, cause these shifts. *St-Laurent et al*. [2013] investigate on-shelf flow of CDW within shelf break troughs in an idealized model of the Bellingshausen Sea and find that a resolution of approximately 1 km is needed to simulate the full range of processes involved. We use a model setup with realistic bathymetry and forcing which covers the entire Amundsen Sea and constraints of computational resources limit our resolution to coarser values. The model results presented in this paper mainly reflect the effect of the mean flow-topography interaction.

[29] The model does capture the cyclonic recirculation in the western part of the trough which is due to vortex stretching at the upstream edge of the trough and pushes the main inflow toward the depression's downstream edge [*St-Laurent et al*., 2013]. Part of the main inflow recirculates first northward to then turn south again along the depression's western flank (Figures 9e and 9f). Noteworthy is also the northward flow along the western end of both model and observed sections (Figures 3, 9c, and 9d). In our simulations, this current transports cooler water from further south on the shelf toward the shelf edge (Figure 11) which leads to the lower temperatures and salinities at the western end of the modeled sections, a feature also present in the observed 2003 section. The 2008 observations confirm that this feature is present at other times as well and is also found further south in the trough. LADCP data from the 2008 section confirms northward flow along the western flank of the 113°W trough [*Wåhlin et al*., 2010]. The absence of cooler water in the western part of the trough in 2006 indicates that the northward flow of cooler shelf waters in the trough may be intermittent. Its role in

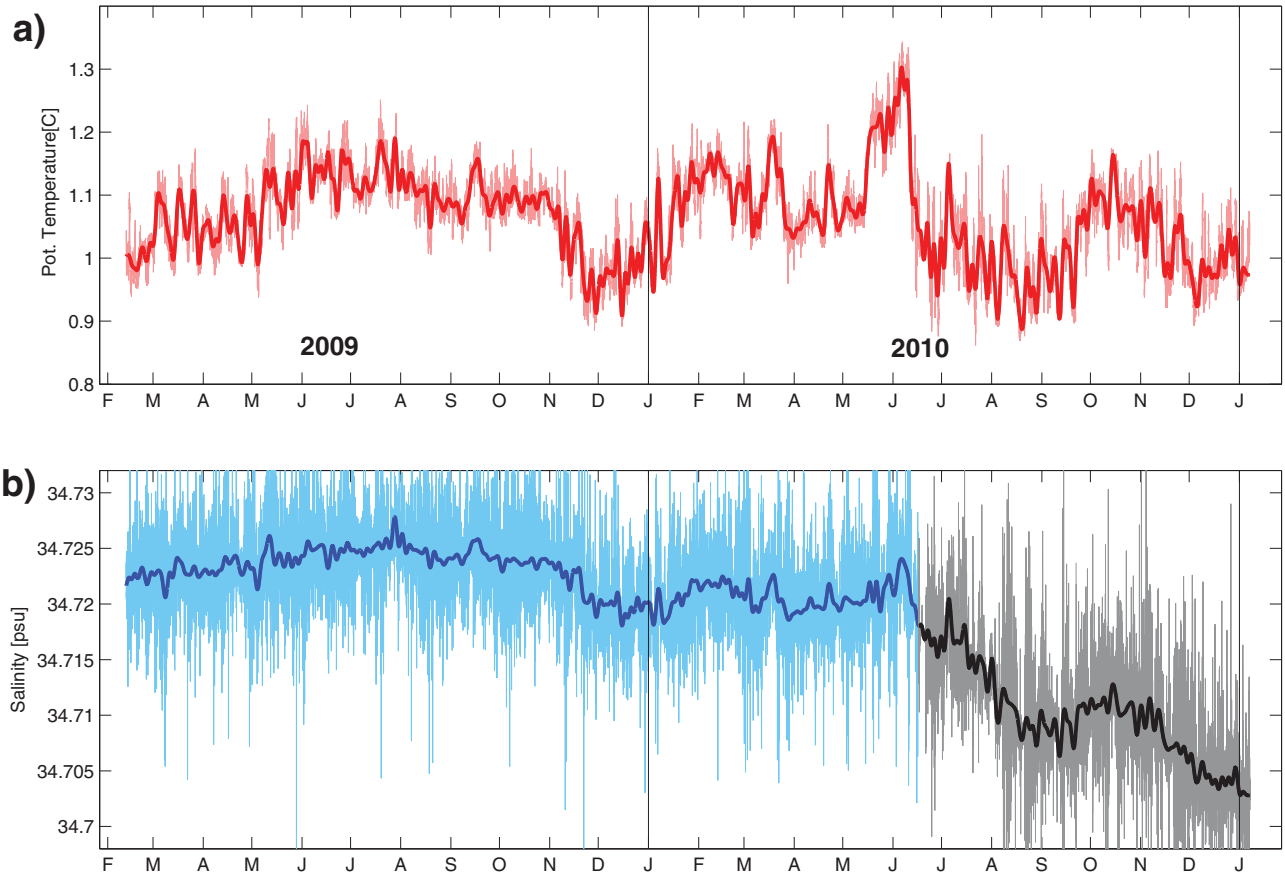

Figure 7. Time series for the mooring sensor at 31 MAB: (a) potential temperature (°C) and (b) salinity (psu). Thin, pale lines show the raw data at 15 min resolution, thicker, darker lines are filtered by a 2 day low-pass filter. The latter part of the salinity record is marked in gray as we suspect sensor drift (see text).

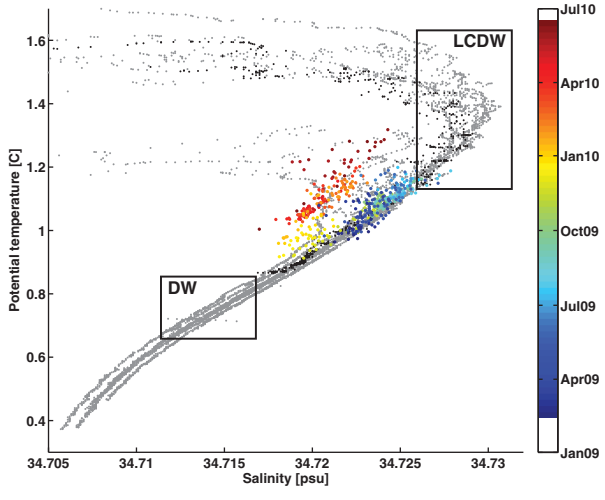

Figure 8. θ-S diagram for the mooring sensor at 31MAB. The gray profiles were made in the trough in 2003 (stations 11–41); black profiles in 2009 (stations 142–144). Mooring data are shown color coded by date and in daily means. The LCDW box marks the Lower Circumpolar Deep Water with salinities above 34.725 [*Orsi et al.*, 1995] and the DW box the underlying Deep Water [*Gouretski*, 1999].

controlling the temperatures of CDW transported onto the shelf has yet to be assessed.

[30] Observed profiles in the trough for 2000 and 2003 show relatively deep WW layers and thermoclines (Figure 2). The thermocline shallows and warms toward 2006 and 2008/2009, and the isolated 1994 station shows a thermocline depth similar to these later years. Stations in Pine Island Bay show similar thermocline variability [*Jacobs et al.*, 2011] and suggest that thermocline depths may covary over the Amundsen Sea continental shelf. The model captures the observed thermocline variability in the trough (Figure 12a), but indicates that there may be variability at time scales shorter than the frequency of the observations. To give us confidence in the modeled interannual variability, we compared the modeled sea ice extent to satellite observations and find that the model captures the variability in sea ice extent well (Figure 12b). A minimum in observed and modeled sea ice extent may explain the warm and fresh surface in February 2006 (Figure 2) in combination with the comparatively early sampling time in early February.

[31] Our model results suggest that the CDW inflow in the 113°W trough and zonal currents along the Amundsen shelf break co-vary strongly (Figure 13a). There is also an area of high correlation with the trough inflow in the zonal surface currents along the shelf break (Figure 13b) which implies that the barotropic current variability seen in the

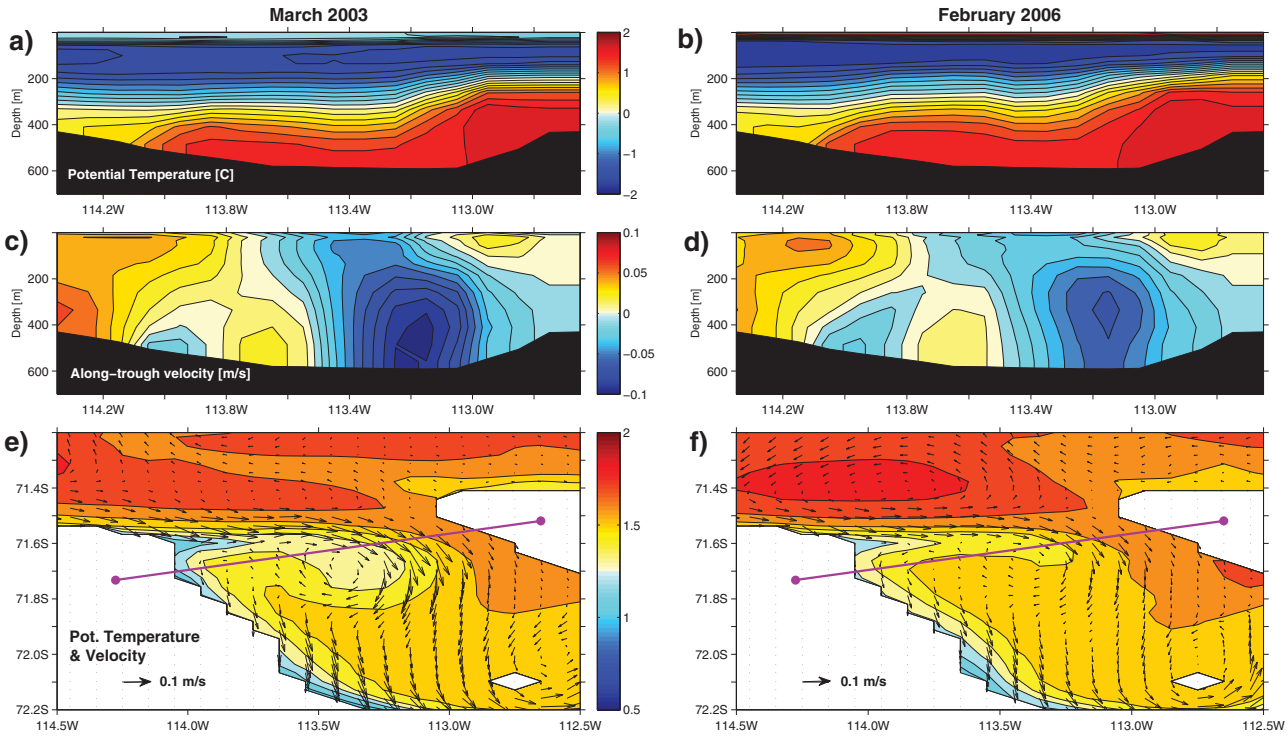

Figure 9. Modeled temperature and currents for the trough region. Monthly means for March 2003 (left) and February 2006 (right). (a and b) Simulated potential temperature (°C) along the track of the 2003 and 2006 cross-trough sections. (c and d) Simulated along-trough velocities for the same section. Note that the model velocities were rotated through the same angle as the observations. (e and f) Potential temperature (°C, color coded) and current velocities (m/s, vectors) at 522.5 m depth. The magenta line marks the position of the cross-trough section.

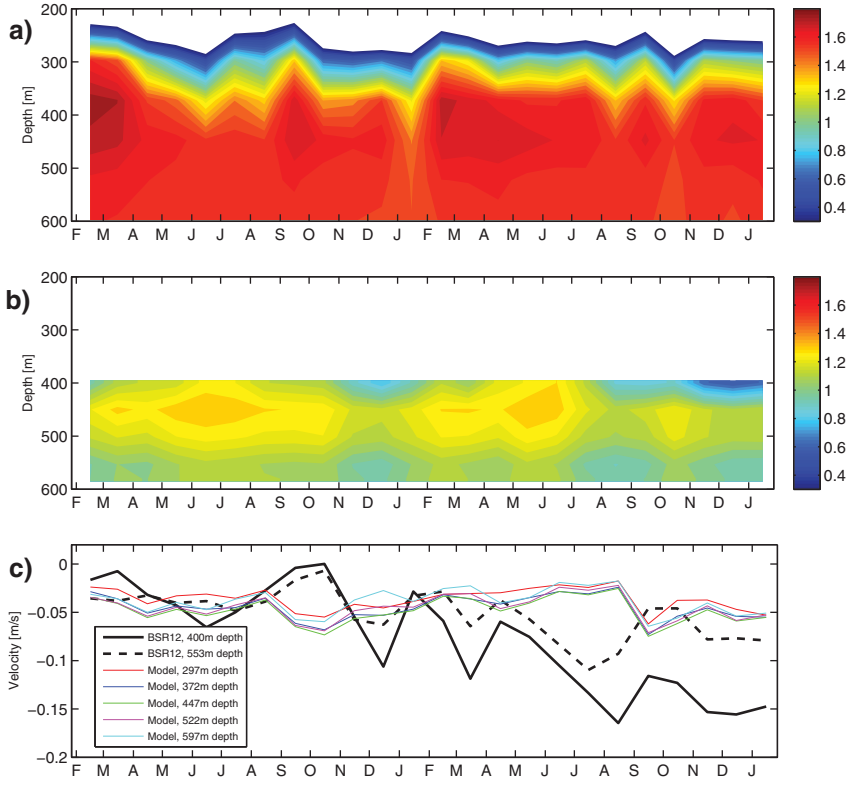

Figure 10. Comparison of simulated and observed potential temperatures at the position of BSR12 from March 2009 to January 2011. (a) Simulated potential temperatures (°C). (b) Observed potential temperatures in monthly means (°C). (c) Observed (black lines, monthly means) and simulated (colored lines, monthly means) along-trough velocities.

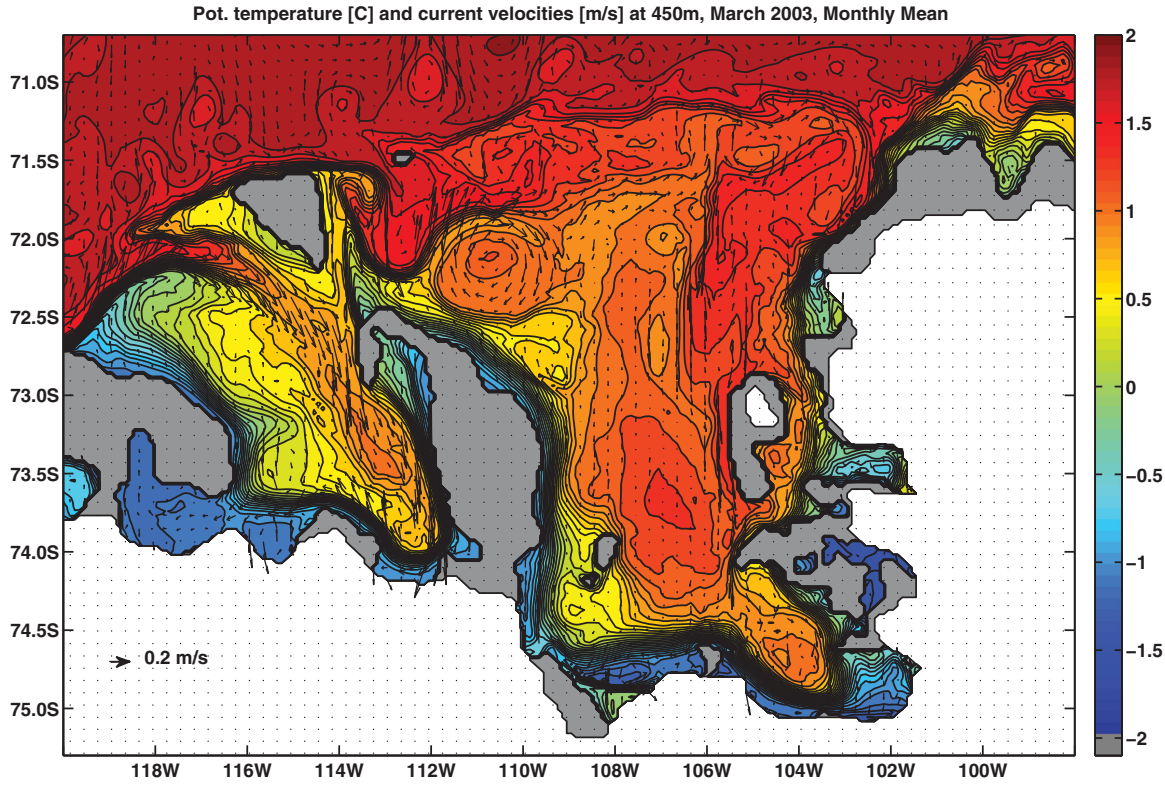

Figure 11. Simulated potential temperature (color coded) and velocities (vectors) at 450 m depth as a monthly mean for March 2003. Land areas are marked white and bathymetry above the layer is shaded gray.

mooring results (Figure 5) is also present in the model and extends beyond the 113°W trough. There are weak, but statistically significant, correlations between the trough inflow and both the zonal and meridional CFSR wind stress component with a maximum lag of 1 day (Figure 13). Enhanced westerly and northerly wind stress both enhance on-shelf flow in the 113°W trough and strengthen the eastward undercurrent system along the shelf break. The location of the area of maximum correlation and the relative importance of the wind stress components for on-shelf transport varies with the time period and time scales considered. The area of maximum correlation of the trough inflow with the zonal wind stress is located at the shelf break between 130 and 85°W (Figures 13c, 13e, and 13g), both for the model and the mooring observations, while that for the meridional wind stress lies just off the shelf at 120°W or on the shelf in the Pine Island Embayment (Figures 13d, 13f, and 13h). This in agreement with a similar analysis by *Wåhlin et al*. [2013] for the trough leading to Getz and Dotson ice shelves and reflects zonal and meridional shifts in the Amundsen Sea low [*Thoma et al*., 2008]. While the zonal winds are generally regarded as the factor controlling the on-shelf transport there may be periods when the meridional wind stress is of equal or greater importance (Figures 13g, 13h, and 14).

5. Discussion

[32] Decadal-scale warming of UCDW has been reported well north of the Amundsen Sea [*Gille*, 2008; *Böning et al*., 2008] and at T_{max} depths in the Ross Gyre west of 140°W [*Jacobs et al*., 2002]. Observations directly north of our study area are too sparse to assess the local extent of such changes, which in any case are small relative to observed thermocline variability in the 113°W trough (e.g., Figures 2 and 4). No warming is apparent within the CDW layer in the depression. *Jacobs et al*. [2011] find a warming of the CDW layer on the inner shelf that is of a similar magnitude to the changes seen north of the shelf break. This small warming may either be due to CDW entering the Amundsen shelf further east or to transport variability and other processes across the shelf.

[33] Variability of the CDW layer in the 113°W trough likely results from proximity to the continental shelf break and slope front, interactions of along-shelf currents with the irregular bathymetry, and from passing storms and fluctuating zonal wind strength and direction. The observations presented by W13 show that the ACC only impinges directly on the shelf break well east of 113°W and that water reaching the shelf in this area is likely to be part of the eastern end of the Ross Gyre. CDW that reaches the shelf break in this region may also be influenced by variable and intermittent eastward extensions of the Ross Gyre [*Assmann and Timmermann*, 2005]. Surface flow at the shelf break is generally to the west overlying an eastward undercurrent at the shelf break that is supported by the southward sloping isopycnals at the shelf break (*W13*) [*Middleton and Cirano*, 1999]. Interaction of this shelf break current with the trough bathymetry causes it to turn into the trough, as also seen in idealized model results by

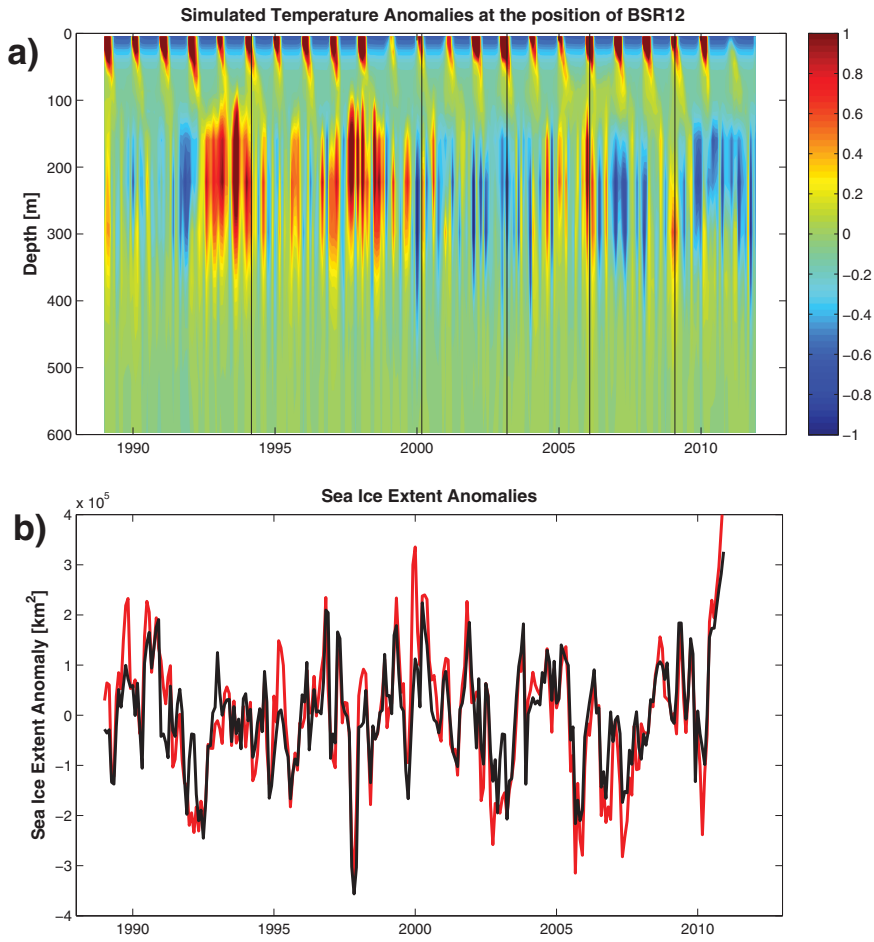

Figure 12. (a) Simulated temperature anomalies for the position of BSR12 in monthly means from 1989 to 2011. Anomalies were calculated by subtracting the 1989–2011 mean for each model depth layer. (b) Simulated (black line) and observed (red line, SSMI) anomalies of sea ice extent (km^2) in the Amundsen Sea (100–125°W).

Klinck [1996] and *St-Laurent et al*. [2013]. This inflow core of CDW can be seen on both cross-trough sections in the central and eastern part of the trough (Figure 3).

[34] At the West Antarctic Peninsula, there is an eastward flowing surface core that weakens with depth, i.e., westward shear with increasing depth [*St-Laurent et al*., 2013]; at the shelf break at 113°W a westward flowing surface core overlies an eastward undercurrent, i.e., eastward shear with increasing depth [*W13*]. These results indicate that vertical current shear at the shelf break is opposite in the Bellingshausen and Amundsen Sea. Both *St-Laurent et al.'s* [2013] model results for the Bellingshausen and our observations and model results for the Amundsen show that the mean flow-topography interaction allows CDW transport onto the shelf. That may imply that the *Klinck* [1996] result that right-bounded flow, i.e., upwelling, will promote cross-shelf break exchange holds regardless of the shear in the water column.

[35] While there is variability in CDW thickness and horizontal structure, both mooring and station data show a persistent presence of CDW in the 113°W trough at seasonal and interannual time scales. The available profiles suggest that the thickness of the CDW layer is usually greater than 150 m and that temperatures within it do not drop below 0.8°C. Observations from the shelf break depression at 117°W that leads to Getz and Dotson ice shelves show considerably larger interannual variability in the thickness and temperature of the CDW within it [*Arneborg et al*., 2012]. Oceanographic observations on the Amundsen Sea continental shelf only commenced in 1994 and *Jenkins et al*. [2010] presented evidence that the grounding line retreat of Pine Island Glacier has been taking place since the 1970s. Thus, the observational period is likely to be too short to have captured the potential changes in oceanic conditions that helped start this process.

[36] The observations show seasonal and interannual variability in thermocline depth and the temperature of the T_{max} core (Figures 2 and 4). Variability in inflow velocities only explains around 10% of the temperature variability in the CDW layer at weekly to monthly time scales, but does dominate the heat transport onto the continental shelf.

[37] An apparent link between temperatures and inflow velocities is that lower CDW temperatures and a deeper thermocline in the mooring record are associated with events of strong on-shelf flow in the CDW layer. This applies to both the cool summer periods and the strong inflow event in August 2010. Θ-S characteristics at the bottom of the trough indicate that the warmer and saltier water found here in winter originates predominantly from

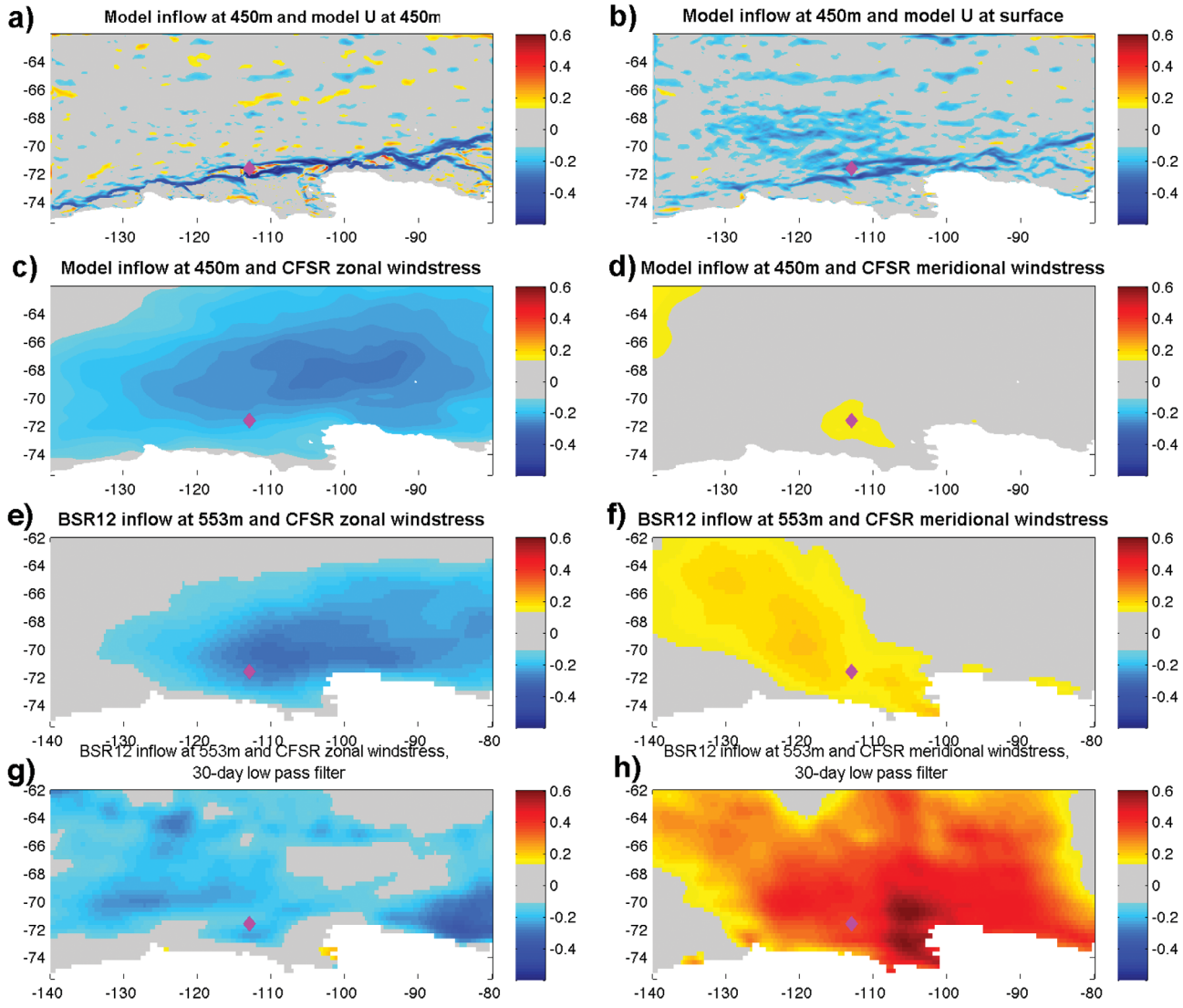

Figure 13. Correlations between CDW inflow velocities and different quantities. Note that inflow velocities are negative for south-eastward flow, i.e., stronger inflow. All model results are monthly means. Gray areas indicate the correlation was not statistically significant at the 95% level. (a) Simulated inflow velocity at 450 m at the mooring position and simulated zonal velocities at 450 m, 1990–2011, zero lag. (b) Simulated inflow velocity at 450 m at the mooring position and simulated zonal velocities at the surface, 1990–2011, zero lag. (c) Simulated inflow velocity at 450 m and zonal CFSR wind stress, 1990–2011, zero lag. (d) Simulated inflow velocity at 450 m and meridional CFSR wind stress, zero lag, 1990–2011. (e) Daily mean observed inflow at 58 MAB (553 m depth) and daily mean zonal CFSR wind stress, lag 1 day, February 2009 to January 2011. (f) Daily mean observed inflow at 58 MAB (553 m depth) and daily mean meridional CFSR wind stress, zero lag, February 2009 to January 2011. (g) Daily mean observed inflow at 58 MAB (553 m depth) and daily mean zonal CFSR wind stress, both smoothed by a 30 day low-pass filter, zero lag, February 2009 to January 2011. (h) Daily mean observed inflow at 58 MAB (553 m depth) and daily mean meridional CFSR wind stress, both smoothed by a 30 day low-pass filter, zero lag, February 2009 to January 2011. The mooring position is marked by the magenta diamond.

LCDW, while the cooler and fresher water found in summer bears deep water characteristics. This implies that as well as a deepening of the thermocline at the top of the CDW layer, deeper waters are being lifted up to a depth where they can flow into the trough, squeezing out the T_{max} of the UCDW remnant. A possible mechanism to explain this is that the deepening of the thermocline enhances the shear within the CDW layer and the strength of the eastward undercurrent leading to upwelling of deeper waters into the trough within a bottom boundary layer.

[38] Similar to the results in *Moffat et al*. [2009], we find that the on-flow of LCDW and the associated heat flux at the bottom of the trough is characterized by a steady background flow that supplies 70% of the heat transport at 113°W. This proportion of heat transported onto the shelf by background flow versus episodic events in our mooring

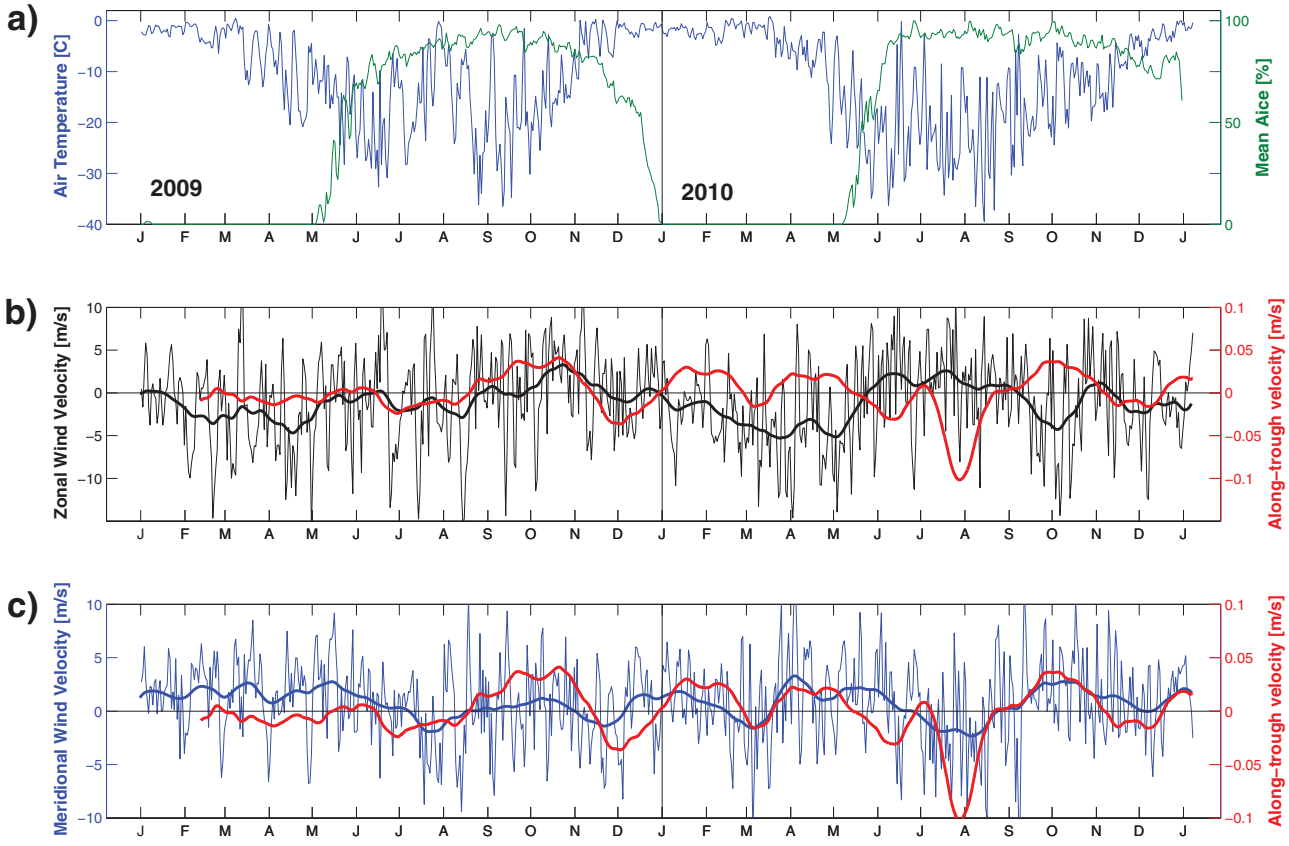

Figure 14. Surface forcing for the trough area (110–117°W, 71–72°S) for 2009 and 2010, the period covered by mooring BSR12. (a) CFSR daily mean air temperature (blue, left scale) and mean sea ice concentration from SSM/I (green, right scale). (b) Zonal CFSR winds (black). Thin line: daily means, bold line: principal component 1 (PC1) of an SSA applied to the daily means (22% of variance explained). (c) Meridional CFSR winds (blue). Thin line: daily mean winds, bold line: PC1 of an SSA applied to the daily mean meridional winds (18% of variance explained). The red line in the two lower plots is the detrended PC1 of the along-trough velocity at 58 MAB on mooring BSR12 (Figure 5).

observations agrees with findings of idealized model studies by *Kämpf* [2009] and *St-Laurent et al*. [2013]. *Martinson and McKee* [2012] find that UCDW eddies modulate the heat content of the CDW layer by up to 20%. Inspection of the velocity time series for the mooring at 113°W (not shown) shows no eddy activity in the LCDW layer and indicates that there may be eddies at 211 MAB. However, since this depth is alternately immersed in the T_{max} core and the thermocline, it is hard to estimate an equivalent.

[39] The temperature records from mooring BSR12 (Figure 4) show a seasonal cycle of warmer autumn, winter, and early spring (March to October) and cooler late spring and summer (November to January). The onset of the thinning of the CDW layer in November coincides with the shift from winter westerlies to summer easterlies in the CFSR data (Figures 1a and 14) which would induce downwelling at the shelf break. However, zonal winds stay on average (Figures 1a) easterly over the 113°W trough until April and thus do not offer an explanation why the observed thermocline begins to shallow in February. A previous model study [*Thoma et al*., 2008; *Steig et al*., 2012] suggested that CDW layer thickness is controlled by the zonal wind variability and in their model the CDW layer thins between November and April when zonal winds over the shelf break are generally easterly (Figure 1a). Zonal winds in 2010 also stay easterly until April (Figure 14) and thus do not offer an explanation why the observed thermocline begins to shallow before this point in time. Decreasing air temperatures over an ice-free ocean surface in March and April (Figure 14) could lead to deep mixing and a deepening of the thermocline. The depth of T_{min} in the observations is commonly around 100 m with no signs that it is ever deeper than 200 m which indicates that local deep mixing is an unlikely candidate to control the seasonal variations in thermocline depth.

[40] The observations in the 113°W trough are predominantly located close to the shelf break. While that makes them extremely valuable for studying the processes that control CDW transport onto the shelf, these same processes make it difficult to use these observations for monitoring interannual changes in on-shelf heat transport. Both ADCP and mooring current meter observations are affected by tides and continental shelf waves that are spatially and temporally complex and hard to estimate. Even though the tidal currents appear to be relatively weak, they limit the use of

ADCP data for referencing geostrophic shear profiles derived from sections that were completed over the same time scale as a tidal cycle, i.e., half a day.

[41] An analysis of observations across the Amundsen shelf by *Nakayama et al*. [2013] indicates that the warmest CDW enters the Amundsen shelf through the eastern trough (Figure 1a), but that the 113°W trough supplies more than half of the cooler, denser CDW that fills the bottom of Pine Island Embayment. This agrees with the model results presented by *Thoma et al*. [2008]. Our model simulations were conducted at higher resolution and thus include a more detailed representation of shelf bathymetry. They indicate that cores of warm CDW enter both troughs at the shelf break (Figure 11) and that the densest CDW is indeed found in the 113°W trough (not shown), but that the main body of CDW that reaches Pine Island Bay enters the shelf through the eastern trough (Figure 11). Depths of the two troughs at the shelf break are similar at around 600 m, but the thermocline deepens westward along the shelf break [*Jacobs et al*., 2012]. Furthermore, it may not be the bottom depth at the shelf break that determines CDW access to the shelf but the sill depths in the southward continuation of these troughs. For the eastern trough this sill depth is around 550 m (all bottom depths from RTOPO1.0.5) [*Timmermann et al*., 2010], while there appear to be two sills of around 520–530 m at 112°W and 109°W, separated by a depression, along the longer shelf continuation of the 113°W trough (Figure 1a). In our model results, the depression separating the two sills is filled with a cyclonic circulation along whose northwestern edge the CDW that entered the shelf through the 113°W trough flows northward and eastward (Figure 11). Bathymetric data coverage in this area is thin [*Nitsche et al*., 2007] and the depression may not necessarily exist in this form. Consequently, our model results may underestimate the influence of the 113°W trough and overestimate that of its eastern neighbor.

[42] The set of observations in the 113°W trough is the most comprehensive at the shelf break in the Amundsen Sea, an area where heavy sea ice makes access difficult, and has allowed us to gain valuable insight into processes governing on-shelf transport of CDW in this area and its variability. Our study of observations in the 113°W trough shows clear signals of variability in CDW temperature structure and thermocline depth at seasonal and interannual time scales. It also shows that ultimately CDW heat transport onto the shelf is controlled by the flow velocity of the CDW rather than its actual temperature. The large interannual variability in thermocline depth raises the question of how coherent these changes are across the Amundsen continental shelf, since the ranges of thermocline depth and draft of ice shelves bordering the Amundsen Sea overlap. Thermocline depth may thus be what ultimately controls the temperature of the water that comes in contact with the ice shelf base and, therefore, the melt rates.

Appendix A: Detiding SADCP Data and Referencing Geostrophic Velocities on the Cross-Trough Sections

[43] Since there is no obvious level of no motion for referencing the geostrophic shear profiles from the cross-trough sections, we used the SADCP data obtained during the 2003 and 2006 cruises for this purpose. We detided the SADCP data and then averaged it for the periods spent stationary at each station and those of steady steaming between the stations. We used several detiding methods and combined the station and underway averages in different ways to test the robustness of the obtained current patterns across the depression and the resulting CDW transport values.

[44] The cross-trough sections are located within 18 km of the shelf break where tides are thought to behave irregularly [*Padman et al*., 2003]. Detiding the SADCP data is necessary, even though tides in the Amundsen Sea are generally thought to be weak (L. Padman, personal communication, 2011), to eliminate a possible bias that predominantly diurnal tides might induce over the cross-trough sections, both of which were completed over a period of about 12 h. To explore related uncertainties we used the following methods to detide the SADCP data for the 2003 and 2006 cruises. We extracted barotropic tidal currents for the two sections from the Circumpolar Antarctic Tidal Simulation 2008 model (CATS2008b) [*Padman et al*., 2002]. CATS2008b includes bathymetric observations taken during the 2003 cruise and the bathymetry in the trough is therefore well represented. We also used a temporal and spatial fit of the O1, K1, M2, and S2 components to the SADCP data using the method described by *Allen* [1995] as applied in *Walker et al*. [2007, 2013]. This was applied to the Amundsen Sea part of each cruise separately and for both cruises combined. We finally extracted the same four tidal components from the current meters at 58 MAB and 211 MAB on mooring BSR12 using T_TIDE (*Pawlowicz et al*. [2002], updated 2011).

[45] Tidal ellipses for the O1, K1, M2, and S2 components for these methods at the BSR12 site (Figure A1) demonstrate the extent of the uncertainty in estimating tidal currents in this region. Application of CATS2008b to the other stations on the cross-trough section (not shown) shows large spatial variability and sensitivity to bathymetry within the trough, at least in a barotropic model. This will affect both the tidal estimates by CATS2008b, which relies on bathymetric observations for correct predictions, and the temporal and spatial fits of the *Allen* [1995] method, which scales tidal currents according to local bottom depth, but does not account for the surrounding bathymetry. Tides diagnosed from the moored current meters may also not be applicable to other parts of the trough. Tides in the trough may not be entirely barotropic, as indicated by the large differences in magnitude between the tides diagnosed from the two current meters on mooring BSR12 (Figure A1). This is corroborated by the results of applying the *Allen* [1995] method to different levels of the SADCP data (not shown).

[46] After detiding, the SADCP data were rotated to obtain the cross-section velocity component. To estimate the uncertainty introduced by choosing either station or underway averaged SADCP data for referencing, we combined the underway and station averaged SADCP cross-section velocities in several different ways. We initially used either the station averaged SADCP data for each station pair or for the underway section between them for all station pairs on the section giving us the first two estimates. We then chose those average underway or station SADCP

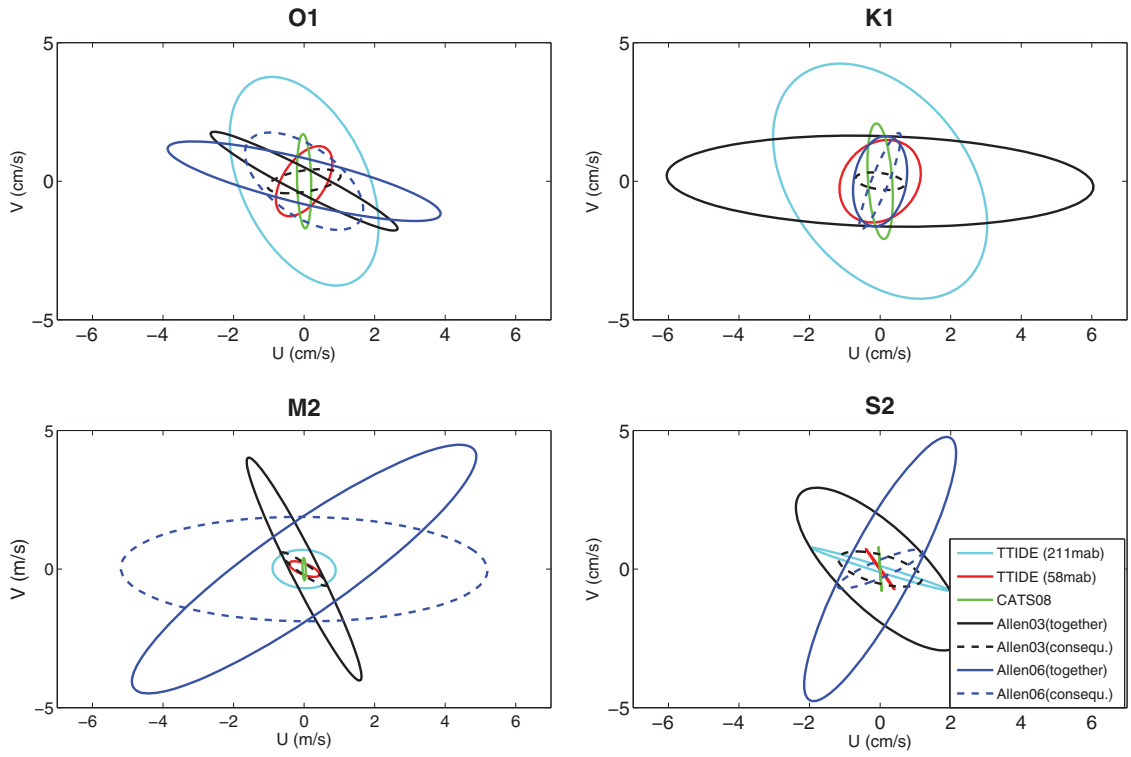

Figure A1. Tidal ellipses for the four major tidal components. Comparison of different detiding methods and tide models. Red T_TIDE [*Pawlowicz et al.*, 2002] applied to current meter 58 MAB, cyan T_TIDE [*Pawlowicz et al.*, 2002] applied to current meter 211 MAB, green CATS2008b, the *Allen* [1995] method applied to the 2003 cruise (black) and 2006 cruise (blue), solid lines denote all four tidal components fitted together, dashed ones consecutively.

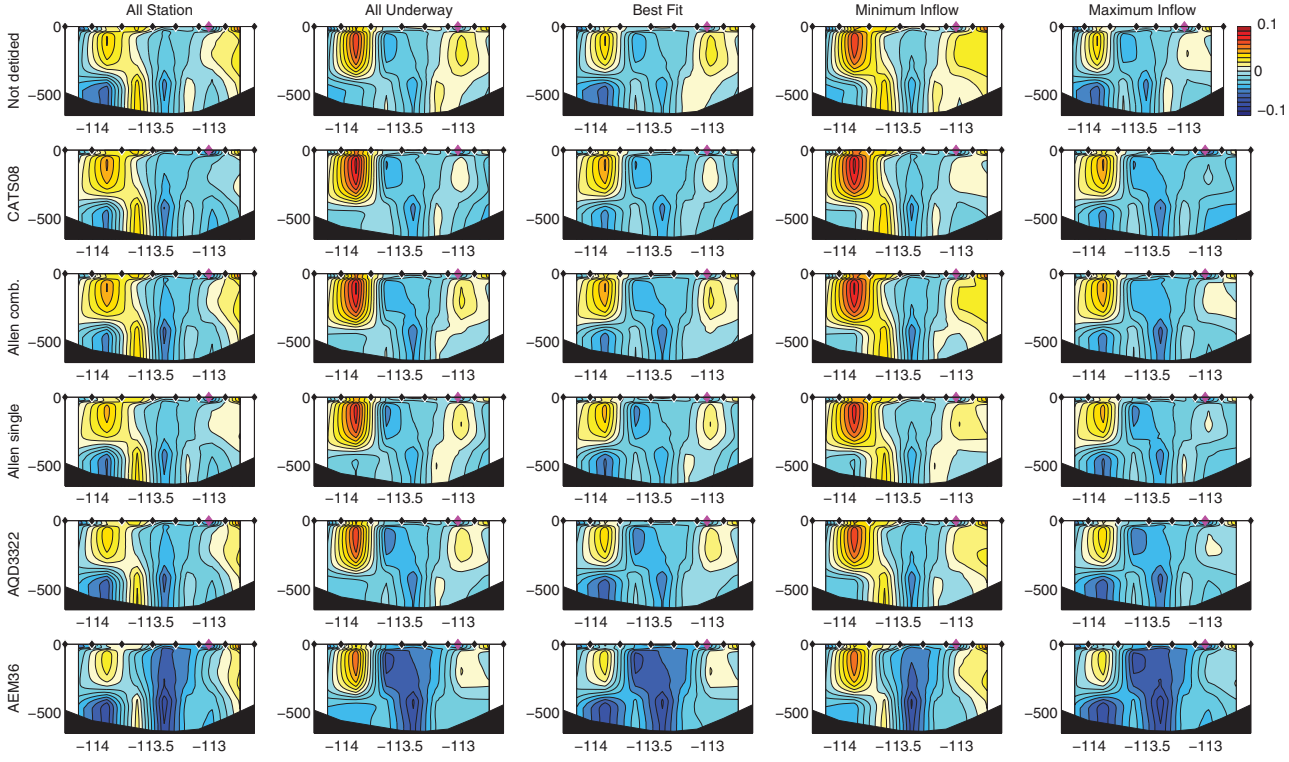

Figure A2. SADCP-referenced geostrophic velocity section for 2003 (positive off the shelf, negative onto the shelf). Each row corresponds to a different detiding method and each column to a different way of combining underway and section averaged SADCP data, as described in Appendix A. Bottom triangles between stations are filled using a constant shear approach. Stations are marked as black diamonds and mooring BSR12 in magenta.

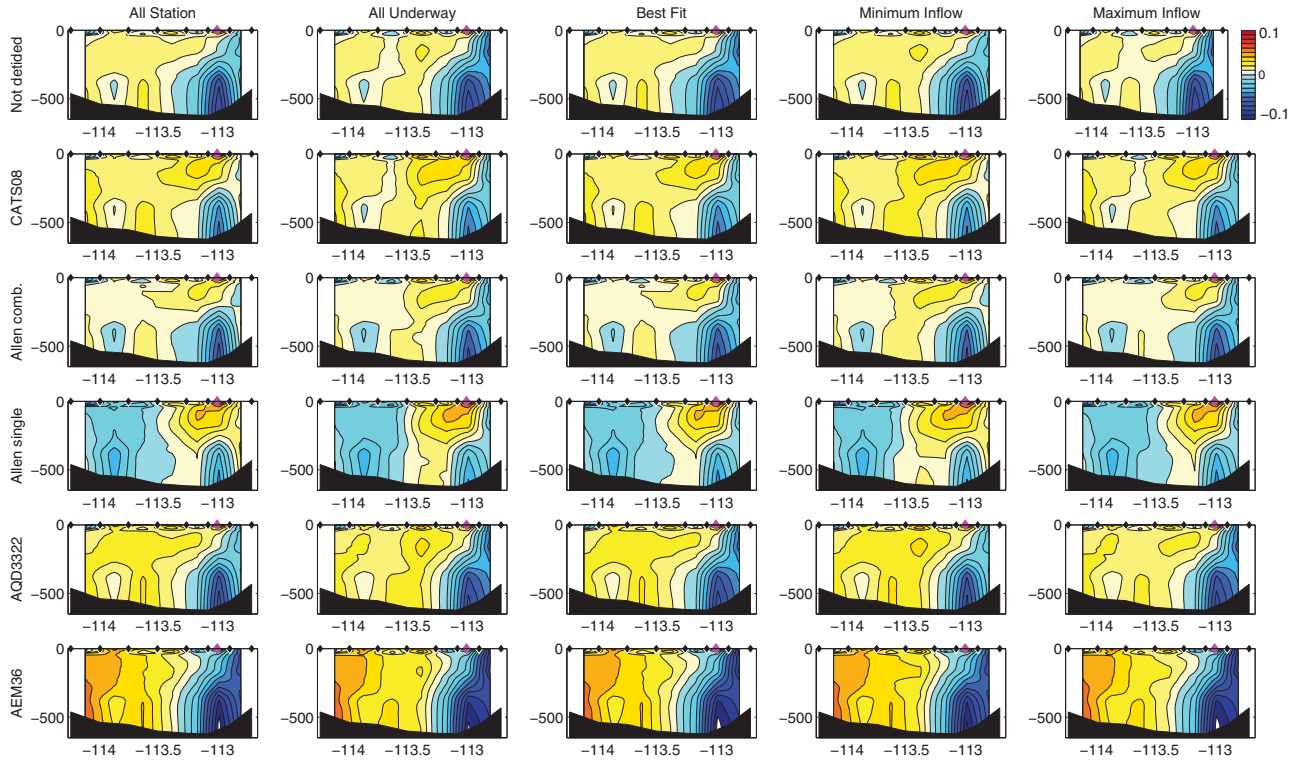

Figure A3. SADCP-referenced geostrophic velocity section for 2006 (positive off the shelf, negative onto the shelf). Each row corresponds to a different detiding method and each column to a different way of combining underway and section averaged SADCP data, as described in Appendix A. Bottom triangles between stations are filled using a constant shear approach. Stations are marked as black diamonds and mooring BSR12 in magenta.

profiles that matched each corresponding geostrophic profile most closely in terms of vertical structure [*Walker et al*., 2007, 2013] for a further estimate. Minimum and maximum CDW transports were identified by choosing those SADCP profiles (underway or station) that minimized or maximized CDW transport onto the shelf. Geostrophic shear profiles were then referenced to the SADCP current averaged between 100 and 300 m.

[47] Figures A2 and A3 show the cross-section velocities for all reference methods for both sections. To calculate velocities in the bottom triangles of the section, we employed both a no shear and constant shear approach. The choice of filling the bottom triangles has a much smaller influence on the calculated CDW volume transports than either the detiding or the ADCP averaging method and is therefore not discussed in detail. While current magnitudes differ, the main features of the current pattern are consistent over all referencing options for both sections. For the 2003 section, the SADCP averaging method exerts a stronger influence on the current pattern and magnitude, while the detiding method dominates for 2006. Since the main features are robust across the different referencing methods and standard deviations do not exceed 0.04 m s^{-1}, we summarize them as a mean in Figure 3.

[48] **Acknowledgments.** The authors would like to thank Martin Losch for helping us to set up MITgcm, Nicolas Bruneau for performing several of the simulations, and Keith Makinson for shedding light on tides at the shelf break. Insightful comments from two anonymous reviewers and Andrey Proshutinsky were very helpful for improving the manuscript. We thank Anna Wåhlin for the use of the Oden data which were received via the NOAA National Oceanographic Data Centre website at http://www.nodc.noaa.gov where the N.B. Palmer data are also available. The 2003 J. C. Ross data set can be obtained from the British Oceanographic Data Centre at http://www.bodc.ac.uk. The 2009 N. B. Palmer observations, including mooring BSR12, were funded by a grant from NSF (ANT 06–32282). Mooring BSR12 was designed by Bruce Huber (LDEO) and deployed and retrieved by Scott Worrilow, Raul Guerrero (LDEO), and Povl Abrahamsen (BAS).

References

Allen, J. T. (1995), Subtidal and tidal currents in the vicinity of the Iceland-Faroes front, *J. Atmos. Oceanic Technol.*, *12*(3), 567–588, doi:1-.1175/1520-0426(1995)012<0567:SATCIT>2.0.CO;2.

Antonov, J. I., D. Seidov, T. P. Boyer, R. A. Locarnini, A. V. Mishonov, H. E. Garcia, O. K. Baranova, M. M. Zweng, and D. R. Johnson (2010), World Ocean Atlas 2009, Volume 2: Salinity, in *NOAA Atlas NESDIS 69*, edited by S. Levitus, 184 pp., U.S. Gov. Print. Off., Washington, D. C.

Arneborg, L., A. K. Wåhlin, G. Björk, B. Liljebladh, and A. H. Orsi (2012), Persistent inflow of warm water onto the central Amundsen shelf, *Nat. Geosci.*, *5*, 876–880, doi:10.1038/NGEO1644.

Assmann, K. M., and R. Timmermann (2005), Variability of dense water formation in the Ross Sea, *Ocean Dyn.*, *55*, 68–87, doi:10.1007/s10236-004-0106-7.

Böning, C. W., A. Dispert, M. Visbeck, S. R. Rintoul, and F. U. Schwarzkopf (2008), The response of the Antarctic Circumpolar Current to recent climate change, *Nat. Geosci.*, *1*, 864–869, doi:10.1038/ngeo362.

Gille, S. T. (2008), Decadal-scale temperature trends in the Southern Hemisphere ocean, *J. Clim.*, *21*, 4749–4765, doi:10.1175/2008JCLI2131.1.

Gouretski, V. V. (1999), The large-scale thermohaline structure of the Ross Gyre, in *Oceanography of the Ross Sea*, edited by G. Spezie and G. M. R. Manzella, pp. 77–102, Springer, Milano.

Hellmer, H. H., S. S. Jacobs, and A. Jenkins (1998), Oceanic erosion of a floating Antarctic glacier in the Amundsen Sea, *AGU Antarct. Res. Ser.*, *75*, 83–99.

Jacobs, S., A. Jenkins, H. Hellmer, C. Giulivi, F. Nitsche, B. Huber, and R. Guerrero (2012), The Amundsen Sea and the Antarctic ice sheet, *Oceanography*, *25*(3), 154–163, doi:10.5670/oceanog.2012.90.

Jacobs, S., C. Giulivi, P. Dutrieux, E. Rignot, F. Nitsche, and J. Mouginot (2013), Getz Ice shelf melting response to changes in ocean forcing, *J. Geophys. Res.*, *118*, doi:10.1002/JGRC.20298.

Jacobs, S. S., H. H. Hellmer, and A. Jenkins (1996), Antarctic ice sheet melting in the southeast Pacific, *Geophys. Res. Lett.*, *23*(9), 957–960.

Jacobs, S. S., C. F. Giulivi, and P. A. Mele (2002), Freshening of the Ross Sea during the late 20th century, *Science*, *297*, 386–389, doi:10.1126/science.1069574.

Jacobs, S. S., A. Jenkins, C. F. Giulivi, and P. Dutrieux (2011), Stronger ocean circulation and increased melting under Pine Island Glacier ice shelf, *Nat. Geosci.*, *4*, 519–523, doi:10.1038/ngeo1188.

Jenkins, A., P. Dutrieux, S. S. Jacobs, S. D. Mc Phail, J. R. Perrett, A. T. Webb, and D. White (2010), Observations beneath Pine Island Glacier in West Antarctica and implications for its retreat, *Nat. Geosci.*, *3*, 468–472, doi:10.1038/NGEO890.

Kämpf, J. (2009), On the interaction of time-variable flows with a shelf-break canyon (2009), *J. Phys. Oceanogr.*, *39*, 248–260, doi:10.1175/2008JPO3753.1.

Klinck, J. M. (1996), Circulation near submarine canyons: A modeling study, *J. Geophys. Res.*, *101*(C1), 1211–1223.

Large, W., J. McWilliams, and S. Doney (1994), Oceanic vertical mixing: A review and a model with nonlocal boundary parametrization, *Rev. Geophys.*, *32*(4), 363–403.

Locarnini, R. A., A. V. Mishonov, J. I. Antonov, T. P. Boyer, H. E. Garcia, O. K. Baranova, M. M. Zweng, and D. R. Johnson (2010), World Ocean Atlas 2009, Volume 1: Temperature, in *NOAA Atlas NESDIS 68*, edited by S. Levitus, 184 pp., U.S. Gov. Print. Off., Washington, D. C.

Losch, M. (2008), Modelling ice shelf cavities in a z-coordinate ocean general circulation model, *J. Geophys. Res.*, *113*, C08043, doi:10.1029/2007JC004368.

Losch, M., D. Menemenlis, J.-M. Campin, P. Heimbach, and C. Hill (2010), On the formulation of sea ice models. Part1: Effects of different solver implications and parameterizations, *Ocean Modell.*, *33*(1–2), 129–144, doi:10.1016/j.ocemod.2009.12.008.

Martinson, D. G., and D. C. McKee (2012), Transport of warm upper circumpolar deep water onto the Western Antarctic Peninsula continental shelf, *Ocean Sci.*, *8*, 433–442, doi:10.5194/os-8–433-2012.

Middleton, J. F., and M. Cirano (1999), Wind-forced downwelling slope currents: A numerical study, *J. Phys. Oceanogr.*, *29*, 1723–1743.

Moffat, C., B. Owens, and R. C. Beardsley (2009), On the characteristics of Circumpolar Deep Water intrusions to the west Antarctic Peninsula Continental Shelf, *J. Geophys. Res.*, *114*, C05017, doi:10.1029/2008JC004955.

Nakayama, Y., M. Schröder, and H. H. Hellmer (2013), From circumpolar deep water to the glacial meltwater plume on the eastern Amundsen Sea shelf, *Deep Sea Res., Part I*, *77*, 50–62, doi:10.1016/j.dsr.2013.04.001.

Nicholls, K. W., S. `sterhus, K. Makinson, T. Gammelsrød, and E. Fahrbach (2009), Ice-ocean processes over the continental shelf of the southern Weddell Sea, Antarctica: A review, *Rev. Geophys.*, *47*, RG3003, doi:10.1029/2007RG000250.

Nitsche, F. O., S. Jacobs, R. D. Larter, and K. Gohl (2007), Bathymetry of the Amundsen Sea continental shelf: Implications for geology, oceanography, and glaciology, *Geochem. Geophys. Geosyst.*, *8*, Q10009, doi:10.1029/2007GC001694.

Orsi, A. H., T. Whitworth III, and W. D. Nowlin Jr. (1995), On the meridional extent and fronts of the Antarctic Circumpolar Current, *Deep Sea Res., Part I*, *42*(5), 641–673.

Padman, L., H. A. Fricker, R. Coleman, S. Howard, and S. Erofeeva (2002), A new tidal model for the Antarctic ice shelves and seas, *Ann. Glaciol.*, *34*, 247–254, doi:1-.3189/172756402781817752.

Padman, L., S. Erofeeva, and I. Joughin (2003), Tides of the Ross Sea and Ross Ice Shelf cavity, *Antarct. Sci.*, *15*(1), 31–40, doi:10.1017/S0954102003001032.

Pawlowicz, R., B. Beardsley, and S. Lentz (2002), Classical tidal harmonic analysis including error estimates in MATLAB using T_TIDE, *Comput. Geosci.*, *28*, 929–937.

Pritchard, H. D., R. J. Arthern, D. G. Vaughan, and L. A. Edwards (2009), Extensive dynamic thinning on the margins of the Greenland and Antarctic ice sheets, *Nature*, *461*, 971–975, doi:10.1038/nature08471.

Rignot, E., and S. S. Jacobs (2002), Rapid bottom melting widespread near Antarctic Ice Sheet grounding lines, *Science*, *296*, 2020–2023, doi:10.1126/science.1070942.

Rignot, E., J. L. Bamber, M. R. van den Broeke, C. Davis, Y. Li, W. J. van de Berg, and E. van Meijgaard (2008), Recent Antarctic ice mass loss from radar interferometry and regional climate modelling, *Nat. Geosci.*, *1*, 106–110, doi:10.1038/ngeo102.

Rignot, E., S. Jacobs, J. Mouginot, and B. Scheuchl (2013), Ice-shelf melting around Antarctica, *Science*, *341*(6143), 266–270, doi:10.1126/science.1235798.

Saha, S., et al. (2010), The NCEP climate forecast system reanalysis, *Bull. Am. Meteorol. Soc.*, *91*, 1015–1057.

Schodlok, M. P., D. Menemenlis, E. Rignot, and M. Studinger (2012), Sensitivity of the ice-shelf/ocean system to the sub-ice-shelf cavity shale measured by NASA IceBridge in Pine Island Glacier, West Antarctica, *Ann. Glaciol.*, *53*(60), doi:10.3189/2012AoG6-A073.

Shepherd, A., D. J. Wingham, A. D. Mansley, and H. F. J. Corr (2001), Inland thinning of Pine Island Glacier, Antarctica, *Science*, *291*, 862–864.

St-Laurent, P., J. M. Klinck, and M. S. Dinniman (2013), On the role of coastal troughs in the circulation of Warm Circumpolar Deep Water on Antarctic Shelves, *J. Phys. Oceanogr.*, *43*, 51–64, doi:10.1175/JPO-D-11–0237.1.

Steig, E. J., Q. DIng, D. S. Battisti, and A. Jenkins (2012), Tropical forcing of Circumpolar Deep Water inflow and outlet glacier thinning in the Amundsen Sea Embayment, West Antarctica, *Ann. Glaciol.*, *53*(60), 19–28, doi:10.3189/2012AoG60A110.

Thoma, M., A. Jenkins, D. Holland, and S. Jacobs (2008), Modelling Circumpolar Deep Water intrusions on the Amundsen Sea continental shelf, Antarctica, *Geophys. Res. Lett.*, *35*, L18602, doi:10.1029/2008GL034939.

Timmermann, R., et al. (2010), A consistent data set of Antarctic ice sheet topography, cavity geometry, and global bathymetry, *Earth Syst. Sci. Data*, *2*(2), 261–273, doi:10.5194/essd-2–261-2010.

Vautard, R., P. Yiou, and M. Ghil (1992), Singular-spectrum analysis—A toolkit for short, noisy chaotic signals, *Physica D*, *58*, 95–126.

Wåhlin, A. K., X. Yuan, G. Björk, and C. Nohr (2010), Inflow of Warm Circumpolar Deep Water in the Central Amundsen Shelf, *J. Phys. Oceanogr.*, *40*, 1427–1434, doi:10.1175/2010JPO4431.1.

Wåhlin, A. K., O. Kalen, L. Arneborg, G. Björk, G. K. Carvajal, H. K. Ha, T. W. Kim, S. H. Lee, J. H. Lee, and C. Stranne (2013), Variability of warm deep water inflow in a submarine trough on the Amundsen shelf, *J. Phys. Oceanogr.*, *43*, 2054–2070, doi:10.1175/JPO-D-12–0157.1.

Walker, D. P., M. A. Brandon, A. Jenkins, J. T. Allen, J. A. Dowdeswell, and J. Evans (2007), Oceanic heat transport onto the Amundsen Sea shelf through a submarine glacial trough, *Geophys. Res. Lett.*, *34*, L02602, doi:10.1029/2006GL028154.

Walker, D. P., A. Jenkins, K. M. Assmann, D. R. Shoosmith, M. A. Brandon (2013), Oceanographic observations at the shelf break of the Amundsen Sea, *J. Geophys. Res.*, *118*, 1–13, doi:10.1002/JGRC.20212.

Whitworth, T., III, A. H. Orsi, S.-J. Kim, W. D. Nowlin Jr., and R. A. Locarnini (1998), Water masses and mixing near the Antarctic slope front, *Antarct. Res. Ser.*, *75*, 1–27.

Wingham, D. J., D. W. Wallis, and A. Shepherd (2009), Spatial and temporal evolution of Pine Island Glacier thinning, 1995–2006, *Geophys. Res. Lett.*, *36*, L17501, doi:10.1029/2009GL039126.

Zwally, H. J., M. B. Giovinetto, J. Li, H. G. Cornejo, M. A. Beckley, A. C. Brenner, J. L. Saba, and D. Yi (2005), Mass changes of the Greenland and Antarctic ice sheets and contributions to sea level rise: 1992–2002, *J. Glaciol.*, *51*(175), 509–527.